Fiber Grating Spectra

Turan Erdogan, *Member, IEEE*

(Invited Paper)

***Abstract*— In this paper, we describe the spectral characteristics that can be achieved in fiber reflection (Bragg) and transmission gratings. Both principles for understanding and tools for designing fiber gratings are emphasized. Examples are given to illustrate the wide variety of optical properties that are possible in fiber gratings. The types of gratings considered include uniform, apodized, chirped, discrete phase-shifted, and superstructure gratings; short-period and long-period gratings; symmetric and tilted gratings; and cladding-mode and radiation-mode coupling gratings.**

***Index Terms*— Distributed feedback devices, gratings, optical fibers, optical fiber communication, optical fiber devices, optical fiber filters.**

I. Introduction

THE fiber phase grating written by ultraviolet light into the core of an optical fiber has developed into a critical component for many applications in fiber-optic communication and sensor systems. These are described in detail in this issue, in numerous previous papers, and in several excellent review articles [1]–[6]. Advantages of fiber gratings over competing technologies include all-fiber geometry, low insertion loss, high return loss or extinction, and potentially low cost. But the most distinguishing feature of fiber gratings is the flexibility they offer for achieving desired spectral characteristics. Numerous physical parameters can be varied, including: induced index change, length, apodization, period chirp, fringe tilt, and whether the grating supports counterpropagating or copropagating coupling at a desired wavelength. By varying these parameters, gratings can be made with normalized bandwidths ($\Delta\lambda/\lambda$) between 0.1 and 10^{-4}, extremely sharp spectral features, and tailorable dispersive characteristics.

In this paper, we focus on the optical properties of fiber phase gratings, in order to provide the reader with both intuition for understanding and tools for designing fiber gratings and related devices. Though many of the concepts developed below are dispersed elsewhere in the literature, it is hoped that by drawing these together and putting them specifically in the context of fiber gratings, the unfamiliar reader will benefit from a concise starting point while the experienced reader will gain a clearer understanding of optical characteristics achievable in fiber-grating components. The discussion below is limited to the linear optical properties of fiber gratings. Although a number of interesting nonlinear-optical properties have been reported recently (see [7] for an excellent review), these are outside the scope of this article. However, the description of linear properties of fiber gratings below is fundamental for understanding these nonlinear properties.

Manuscript received April 8, 1997; revised April 24, 1997. This work was supported by the National Science Foundation (award ECS-9 502 670) and the Alfred P. Sloan Foundation.

The author is with The Institute of Optics, University of Rochester, Rochester, NY 14627 USA.

Publisher Item Identifier S 0733-8724(97)05942-2.

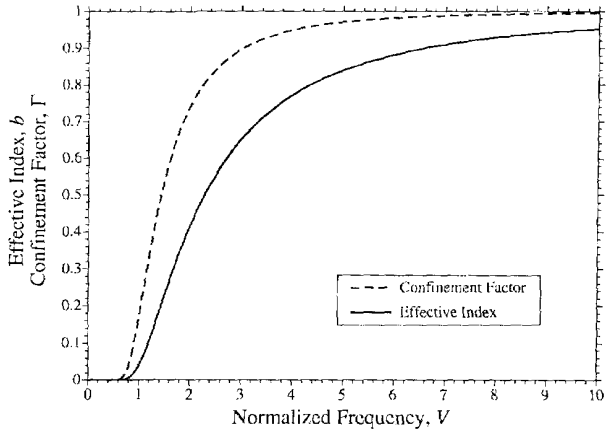

Fig. 1. Effective index parameter b and core confinement factor Γ versus normalized frequency V for the LP_{01} mode of a step index fiber.

Fiber phase gratings are produced by exposing an optical fiber to a spatially varying pattern of ultraviolet intensity. Here we assume for simplicity that what results is a perturbation to the effective refractive index n_{eff} of the guided mode(s) of interest, described by

$$\delta n_{\text{eff}}(z) = \overline{\delta n}_{\text{eff}}(z)\left\{1 + v\cos\left[\frac{2\pi}{\Lambda}z + \phi(z)\right]\right\} \quad (1)$$

where $\overline{\delta n}_{\text{eff}}$ is the "dc" index change spatially averaged over a grating period, v is the fringe visibility of the index change, Λ is the nominal period, and $\phi(z)$ describes grating chirp. If the fiber has a step-index profile and an induced index change $\delta n_{co}(z)$ is created uniformly across the core, then we find that $\delta n_{\text{eff}} \cong \Gamma\delta n_{co}$ where Γ is the core power confinement factor for the mode of interest. For example, Fig. 1 shows the confinement factor Γ and the effective index parameter b for the LP_{01} mode. For $LP_{l\mu}$ modes, b is a solution to the dispersion relation [8]

$$V\sqrt{1-b}\,\frac{J_{l-1}\left(V\sqrt{1-b}\right)}{J_l\left(V\sqrt{1-b}\right)} = -V\sqrt{b}\,\frac{K_{l-1}\left(V\sqrt{b}\right)}{K_l\left(V\sqrt{b}\right)} \quad (2)$$

where l is the azimuthal order of the mode and $V = (2\pi/\lambda)a\sqrt{n_{co}^2 - n_{cl}^2}$ is a normalized frequency, with a

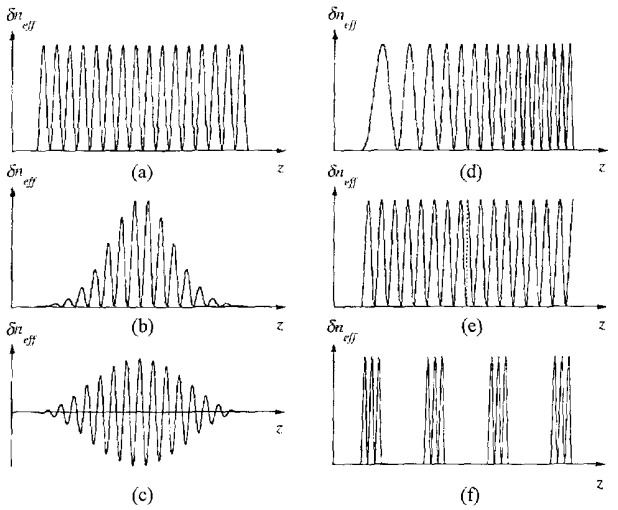

Fig. 2. Common types of fiber gratings as classified by variation of the induced index change along the fiber axis, including (a) uniform with positive-only index change, (b) Gaussian-apodized, (c) raised-cosine-apodized with zero-dc index change, (d) chirped, (e) discrete phase shift (of π), and (f) superstructure.

the core radius, n_{co} the core index and n_{cl} the cladding index. The effective index is related to b through $b = (n_{\text{eff}}^2 - n_{cl}^2)/(n_{\text{co}}^2 - n_{cl}^2)$. Once V and b are known, Γ can be determined from

$$\Gamma = \frac{b^2}{V^2}\left[1 - \frac{J_l^2(V\sqrt{1-b})}{J_{l+1}(V\sqrt{1-b})J_{l-1}(V\sqrt{1-b})}\right]. \quad (3)$$

The optical properties of a fiber grating are essentially determined by the variation of the induced index change δn_{eff} along the fiber axis z. Fig. 2 illustrates some common variations that are discussed in this paper. The terminology used to describe these is given in the figure caption. For illustrative purposes the size of the grating period relative to the grating length has been greatly exaggerated.

The remainder of this paper is organized as follows. In Section II, we examine the optical properties of uniform fiber gratings when coupling occurs between only two modes, since this case yields simple solutions for the reflection and transmission. The coupled-mode theory that is a vital tool for understanding gratings is introduced in this section, and some basic design rules-of-thumb applicable to all fiber gratings are established. In Section III, the analysis is extended to include two-mode coupling in nonuniform gratings, including apodized, chirped, phase-shifted, and superstructure gratings. Numerical techniques for analyzing these are discussed, and examples are provided. In Section IV, we briefly consider the effects of grating tilt, or blazing, on the optical properties of Bragg gratings. Then, in Section V, we discuss the optical properties that result from coupling to a multiplicity of cladding modes, and in Section VI coupling to the continuum of radiation modes is considered. Finally, concluding remarks are given in Section VII.

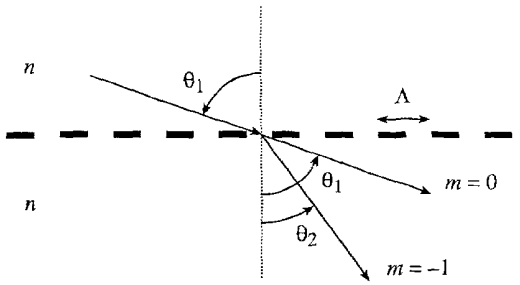

Fig. 3. The diffraction of a light wave by a grating.

II. Two-Mode Coupling in Uniform Gratings

A. Resonant Wavelength for Grating Diffraction

In Section II, we focus on the simple case of coupling between two fiber modes by a uniform grating. Before we develop the quantitative analysis using coupled-mode theory, it is helpful to consider a qualitative picture of the basic interactions of interest. A fiber grating is simply an optical diffraction grating, and thus its effect upon a light wave incident on the grating at an angle θ_1 can be described by the familiar grating equation [9]

$$n \sin \theta_2 = n \sin \theta_1 + m\frac{\lambda}{\Lambda} \quad (4)$$

where θ_2 is the angle of the diffracted wave and the integer m determines the diffraction order (see Fig. 3). This equation predicts only the directions θ_2 into which constructive interference occurs, but it is nevertheless capable of determining the wavelength at which a fiber grating most efficiently couples light between two modes.

Fiber gratings can be broadly classified into two types: *Bragg gratings* (also called *reflection* and *short-period* gratings), in which coupling occurs between modes traveling in opposite directions; and *transmission gratings* (also called *long-period* gratings), in which the coupling is between modes traveling in the same direction. Fig. 4(a) illustrates reflection by a Bragg grating of a mode with a bounce angle of θ_1 into the same mode traveling in the opposite direction with a bounce angle of $\theta_2 = -\theta_1$. Since the mode propagation constant β is simply $\beta = (2\pi/\lambda)n_{\text{eff}}$ where $n_{\text{eff}} = n_{co} \sin \theta$, we may rewrite (4) for guided modes as

$$\beta_2 = \beta_1 + m\frac{2\pi}{\Lambda}. \quad (5)$$

For first-order diffraction, which usually dominates in a fiber grating, $m = -1$. This condition is illustrated on the β axis shown below the fiber. The solid circles represent bound core modes ($n_{cl} < n_{\text{eff}} < n_{co}$), the open circles represent cladding modes ($1 < n_{\text{eff}} < n_{cl}$), and the hatched regions represent the continuum of radiation modes. Negative β values describe modes that propagate in the $-z$ direction. By using (5) and recognizing $\beta_2 < 0$, we find that the resonant wavelength for reflection of a mode of index $n_{eff,1}$ into a mode of index $n_{eff,2}$ is

$$\lambda = (n_{eff,1} + n_{eff,2})\Lambda. \quad (6)$$

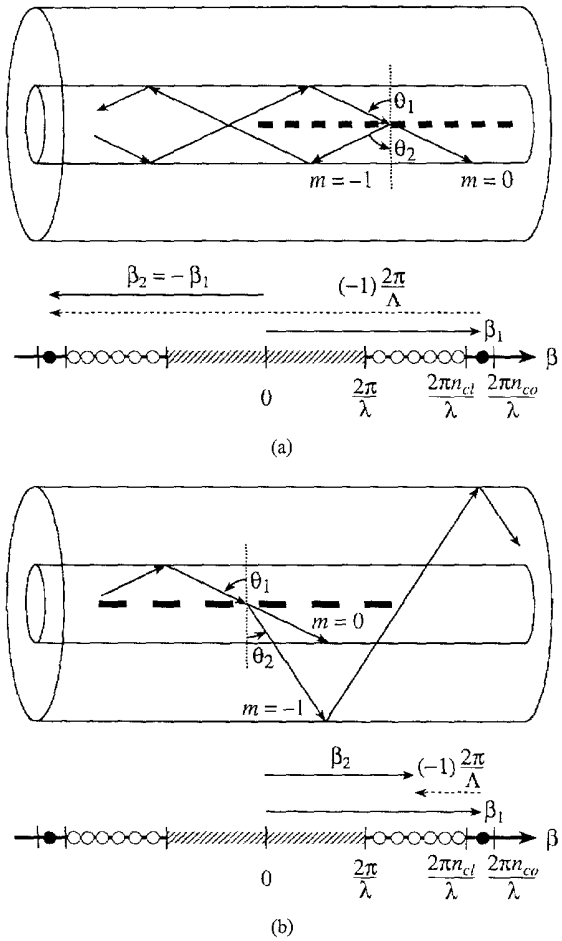

Fig. 4. Ray-optic illustration of (a) core-mode Bragg reflection by a fiber Bragg grating and (b) cladding-mode coupling by a fiber transmission grating. The β axes below each diagram demonstrate the grating condition in (5) for $m = -1$.

If the two modes are identical, we get the familiar result for Bragg reflection: $\lambda = 2n_{\text{eff}}\Lambda$.

Diffraction by a transmission grating of a mode with a bounce angle of θ_1 into a co-propagating mode with a bounce angle of θ_2 is illustrated in Fig. 4(b). In this illustration the first mode is a core mode while the second is a cladding mode. Since here $\beta_2 > 0$, (5) predicts the resonant wavelength for a transmission grating as

$$\lambda = (n_{eff,1} - n_{eff,2})\Lambda. \tag{7}$$

For copropagating coupling at a given wavelength, evidently a much longer grating period Λ is required than for counter-propagating coupling.

B. Coupled-Mode Theory

Coupled-mode theory is a good tool for obtaining quantitative information about the diffraction efficiency and spectral dependence of fiber gratings. While other techniques are available, here we consider only coupled-mode theory since it is straightforward, it is intuitive, and it accurately models the optical properties of most fiber gratings of interest. We do not provide a derivation of coupled-mode theory, as this is detailed in numerous articles and texts [10], [11]. Our notation follows most closely that of Kogelnik [11]. In the ideal-mode approximation to coupled-mode theory, we assume that the transverse component of the electric field can be written as a superposition of the ideal modes labeled j (i.e., the modes in an ideal waveguide with no grating perturbation), such that

$$\vec{E}_t(x, y, z, t) = \sum_j [A_j(z)\exp(i\beta_j z) + B_j(z)\exp(-i\beta_j z)] \cdot \vec{e}_{jt}(x, y)\exp(-i\omega t) \tag{8}$$

where $A_j(z)$ and $B_j(z)$ are slowly varying amplitudes of the jth mode traveling in the $+z$ and $-z$ directions, respectively. The transverse mode fields $\vec{e}_{jt}(x, y)$ might describe the bound-core or radiation LP modes, as given in [8], or they might describe cladding modes. While the modes are orthogonal in an ideal waveguide and hence, do not exchange energy, the presence of a dielectric perturbation causes the modes to be coupled such that the amplitudes A_j and B_j of the jth mode evolve along the z axis according to

$$\frac{dA_j}{dz} = i\sum_k A_k(K^t_{kj} + K^z_{kj})\exp[i(\beta_k - \beta_j)z] + i\sum_k B_k(K^t_{kj} - K^z_{kj})\exp[-i(\beta_k + \beta_j)z] \tag{9}$$

$$\frac{dB_j}{dz} = -i\sum_k A_k(K^t_{kj} - K^z_{kj})\exp[i(\beta_k + \beta_j)z] - i\sum_k B_k(K^t_{kj} + K^z_{kj})\exp[-i(\beta_k - \beta_j)z]. \tag{10}$$

In (9) and (10), $K^t_{kj}(z)$ is the transverse coupling coefficient between modes j and k given by

$$K^t_{kj}(z) = \frac{\omega}{4}\iint_\infty dx\,dy\,\Delta\varepsilon(x, y, z)\,\vec{e}_{kt}(x, y)\cdot\vec{e}^*_{jt}(x, y) \tag{11}$$

where $\Delta\varepsilon$ is the perturbation to the permittivity, approximately $\Delta\varepsilon \cong 2n\delta n$ when $\delta n \ll n$. The longitudinal coefficient $K^z_{kj}(z)$ is analogous to $K^t_{kj}(z)$, but generally $K^z_{kj}(z) \ll K^t_{kj}(z)$ for fiber modes, and thus this coefficient is usually neglected.

In most fiber gratings the induced index change $\delta n(x, y, z)$ is approximately uniform across the core and nonexistent outside the core. We can thus describe the core index by an expression similar to (1), but with $\overline{\delta n}_{\text{eff}}(z)$ replaced by $\overline{\delta n}_{co}(z)$. If we define two new coefficients

$$\sigma_{kj}(z) = \frac{\omega\, n_{co}}{2}\overline{\delta n}_{co}(z)\iint_{\text{core}} dx\,dy\,\vec{e}_{kt}(x, y)\cdot\vec{e}^*_{jt}(x, y) \tag{12}$$

$$\kappa_{kj}(z) = \frac{v}{2}\sigma_{kj}(z) \tag{13}$$

where σ is a "dc" (period-averaged) coupling coefficient and κ is an "AC" coupling coefficient, then the general coupling

coefficient can be written

$$K_{kj}^{t}(z) = \sigma_{kj}(z) + 2\kappa_{kj}(z) \cos\left[\frac{2\pi}{\Lambda} z + \phi(z)\right]. \quad (14)$$

Equations (9)–(14) are the coupled-mode equations that we use to describe fiber-grating spectra below.

C. Bragg Gratings

Near the wavelength for which reflection of a mode of amplitude $A(z)$ into an identical counter-propagating mode of amplitude $B(z)$ is the dominant interaction in a Bragg grating, (9) and (10) may be simplified by retaining only terms that involve the amplitudes of the particular mode, and then making the "synchronous approximation" [11]. The latter amounts to neglecting terms on the right-hand sides of the differential equations that contain a rapidly oscillating z dependence, since these contribute little to the growth and decay of the amplitudes. The resulting equations can be written

$$\frac{dR}{dz} = i\hat{\sigma}R(z) + i\kappa S(z) \quad (15)$$

$$\frac{dS}{dz} = -i\hat{\sigma}S(z) - i\kappa^{*}R(z) \quad (16)$$

where the amplitudes R and S are $R(z) \equiv A(z)\exp(i\delta z - \phi/2)$ and $S(z) \equiv B(z)\exp(-i\delta z + \phi/2)$. In these equations κ is the "AC" coupling coefficient from (13) and $\hat{\sigma}$ is a general "dc" self-coupling coefficient defined as

$$\hat{\sigma} \equiv \delta + \sigma - \frac{1}{2}\frac{d\phi}{dz}. \quad (17)$$

The detuning δ, which is independent of z for all gratings, is defined to be

$$\begin{aligned}\delta &\equiv \beta - \frac{\pi}{\Lambda} \\ &= \beta - \beta_D \\ &= 2\pi n_{\text{eff}}\left(\frac{1}{\lambda} - \frac{1}{\lambda_D}\right)\end{aligned} \quad (18)$$

where $\lambda_D \equiv 2n_{\text{eff}}\Lambda$ is the "design wavelength" for Bragg scattering by an infinitesimally weak grating ($\delta n_{\text{eff}} \to 0$) with a period Λ. Note when $\delta = 0$ we find $\lambda = 2n_{\text{eff}}\Lambda$, the Bragg condition predicted by the qualitative grating picture above. The "dc" coupling coefficient σ is defined in (12). Absorption loss in the grating can be described by a complex coefficient σ, where the power loss coefficient is $\alpha = 2\,\text{Im}(\sigma)$. Light not reflected by the grating experiences a transmission loss of $10\log_{10}(e)\alpha$ dB/cm. Finally, the derivative $(1/2)d\phi/dz$ describes possible chirp of the grating period, where $\phi(z)$ is defined through (1) or (14).

For a single-mode Bragg reflection grating, we find the following simple relations:

$$\sigma = \frac{2\pi}{\lambda}\overline{\delta n}_{\text{eff}} \quad (19)$$

$$\begin{aligned}\kappa &= \kappa^{*} \\ &= \frac{\pi}{\lambda} v\overline{\delta n}_{\text{eff}}.\end{aligned} \quad (20)$$

If the grating is uniform along z, then $\overline{\delta n}_{\text{eff}}$ is a constant and $d\phi/dz = 0$, and thus κ, σ, and $\hat{\sigma}$ are constants. Thus, (15) and (16) are coupled first-order ordinary differential equations with constant coefficients, for which closed-form solutions can be found when appropriate boundary conditions are specified. The reflectivity of a uniform fiber grating of length L can be found by assuming a forward-going wave incident from $z = -\infty$ [say $R(-L/2) = 1$] and requiring that no backward-going wave exists for $z \geq L/2$ [i.e., $S(L/2) = 0$]. The amplitude and power reflection coefficients $\rho = S(-L/2)/R(-L/2)$ and $r = |\rho|^2$, respectively, can then be shown to be [10], [11]

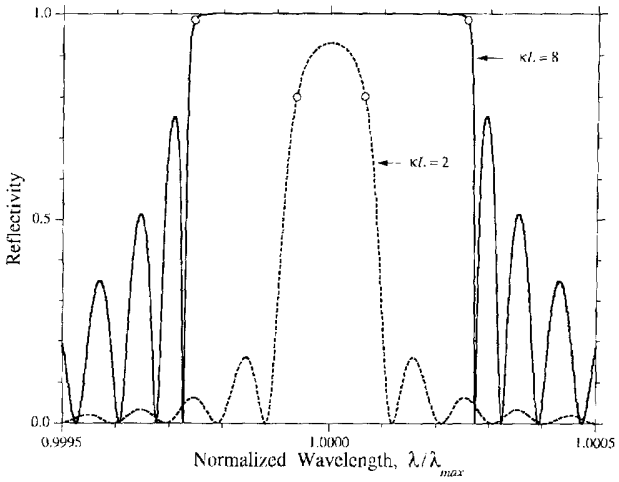

Fig. 5. Reflection spectra versus normalized wavelength for Bragg reflection in uniform gratings with $\kappa L = 2$ (dashed line) and $\kappa L = 8$ (solid line).

$$\rho = \frac{-\kappa \sinh\left(\sqrt{\kappa^2 - \hat{\sigma}^2}L\right)}{\hat{\sigma}\sinh\left(\sqrt{\kappa^2 - \hat{\sigma}^2}L\right) + i\sqrt{\kappa^2 - \hat{\sigma}^2}\cosh\left(\sqrt{\kappa^2 - \hat{\sigma}^2}L\right)} \quad (21)$$

and

$$r = \frac{\sinh^2\left(\sqrt{\kappa^2 - \hat{\sigma}^2}L\right)}{\cosh^2\left(\sqrt{\kappa^2 - \hat{\sigma}^2}L\right) - \dfrac{\hat{\sigma}^2}{\kappa^2}}. \quad (22)$$

A number of interesting features of fiber Bragg gratings can be seen from these results. Typical examples of the power reflectivity r for uniform gratings with $\kappa L = 2$ and $\kappa L = 8$ are shown in Fig. 5, plotted versus the normalized wavelength

$$\frac{\lambda}{\lambda_{\max}} = \frac{1}{1 + \dfrac{\hat{\sigma}L}{\pi N}} \quad (23)$$

where N is the total number of grating periods ($N = L/\Lambda$), here chosen to be $N = 10\,000$, and $\lambda_{\max}$ is the wavelength at which maximum reflectivity occurs. If N were larger or smaller, the reflection bandwidth would be narrower or broader, respectively, for a given value of κL. From (22), we find the maximum reflectivity $r_{\max}$ for a Bragg grating is

$$r_{\max} = \tanh^2(\kappa L) \quad (24)$$

and it occurs when $\hat{\sigma} = 0$, or at the wavelength

$$\lambda_{\max} = \left(1 + \frac{\overline{\delta n}_{\text{eff}}}{n_{\text{eff}}}\right)\lambda_D. \quad (25)$$

The points on these plots denoted by open circles indicate the "band edges," or the points at the edges of the "band gap"; defined such that $|\hat{\sigma}| < \kappa$. Inside the band gap, the amplitudes $R(z)$ and $S(z)$ grow and decay exponentially along z; outside the band gap they evolve sinusoidally. The reflectivity at the band edges is

$$r_{\text{band edge}} = \frac{(\kappa L)^2}{1+(\kappa L)^2} \tag{26}$$

and the band edges occur at the wavelengths

$$\lambda_{\text{band edge}} = \lambda_{\max} \pm \frac{v\overline{\delta n}_{\text{eff}}}{2n_{\text{eff}}} \lambda_D. \tag{27}$$

From (27) the normalized bandwidth of a Bragg grating as measured at the band edges is simply

$$\frac{\Delta\lambda_{\text{band edge}}}{\lambda} = \frac{v\overline{\delta n}_{\text{eff}}}{n_{\text{eff}}} \tag{28}$$

where $v\overline{\delta n}_{\text{eff}}$ is simply the "AC" part of the induced index change.

A more readily measurable bandwidth for a uniform Bragg grating is that between the first zeros on either side of the maximum reflectivity. Looking at the excursion of $\hat{\sigma}$ from $\hat{\sigma} = 0$ that causes the numerator in (22) to go to zero, we find

$$\frac{\Delta\lambda_0}{\lambda} = \frac{v\overline{\delta n}_{\text{eff}}}{n_{\text{eff}}} \sqrt{1+\left(\frac{\lambda_D}{v\overline{\delta n}_{\text{eff}} L}\right)^2}. \tag{29}$$

In the "weak-grating limit," for which $v\overline{\delta n}_{\text{eff}}$ is very small, we find

$$\frac{\Delta\lambda_0}{\lambda} \to \frac{\lambda_D}{n_{\text{eff}} L} = \frac{2}{N} \qquad \left(v\overline{\delta n}_{\text{eff}} \ll \frac{\lambda_D}{L}\right) \tag{30}$$

the bandwidth of weak gratings is said to be "length-limited." However, in the "strong-grating limit," we find

$$\frac{\Delta\lambda_0}{\lambda} \to \frac{v\overline{\delta n}_{\text{eff}}}{n_{\text{eff}}} \qquad \left(v\overline{\delta n}_{\text{eff}} \gg \frac{\lambda_D}{L}\right). \tag{31}$$

In strong gratings, the light does not penetrate the full length of the grating, and thus the bandwidth is independent of length and directly proportional to the induced index change. For strong gratings the bandwidth is similar whether measured at the band edges, at the first zeros, or as the full-width-at-half-maximum (FWHM).

To compare the theory to an experimental measurement, Fig. 6 shows the measured (dots) and calculated (line) reflection from a 1.0-mm-long uniform grating with a design wavelength of 1558 nm and an induced index change of $v\overline{\delta n}_{\text{eff}} = 8 \times 10^{-4}$, thus yielding $\kappa L = 1.64$.

Recently, there is growing interest in the dispersive properties of fiber Bragg gratings for applications such as dispersion compensation, pulse shaping, and fiber and semiconductor laser components. Although many of these rely on the ability to tailor the dispersion in the nonuniform gratings discussed in Section III, here we introduce the basis for determining delay and dispersion from the known (complex) reflectivity of a Bragg grating. The group delay and dispersion of the reflected light can be determined from the phase of the amplitude

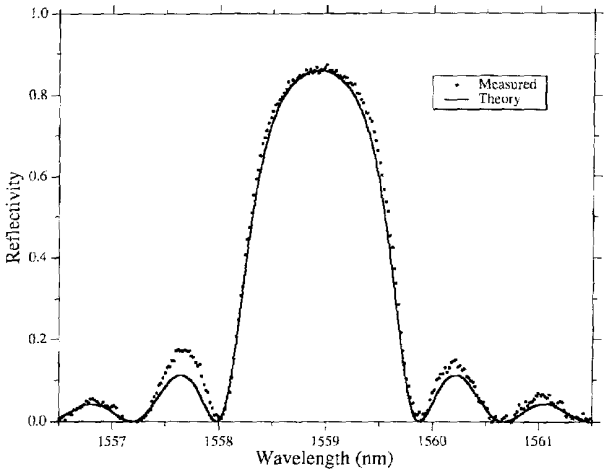

Fig. 6. Measured (dots) and calculated (line) reflection spectra for Bragg reflection in a 1-mm-long uniform grating with $\kappa L = 1.64$.

reflection coefficient ρ in (21). If we denote $\theta_\rho \equiv phase(\rho)$, then at a local frequency ω_0 we may expand θ_ρ in a Taylor series about ω_0. Since the first derivative $d\theta_\rho/d\omega$is directly proportional to the frequency ω, this quantity can be identified as a time delay. Thus, the delay time τ_ρ for light reflected off of a grating is

$$\tau_\rho = \frac{d\theta_\rho}{d\omega} = -\frac{\lambda^2}{2\pi c}\frac{d\theta_\rho}{d\lambda}. \tag{32}$$

τ_ρ is usually given in units of picoseconds. Fig. 7 shows the delay τ_ρ calculated for the two example gratings from Fig. 5. Here the grating length is $L = 1$ cm, the Design wavelength is $\lambda_D = 1550$ nm, $n_{\text{eff}} = 1.45$, and the fringe visibility is $v = 1$. For the weaker grating in Fig. 7(a), $\overline{\delta n}_{\text{eff}} = 1 \times 10^{-4}$, while for the stronger grating in Fig. 7(b), $\overline{\delta n}_{\text{eff}} = 4 \times 10^{-4}$. We see that for unchirped uniform gratings both the reflectivity and the delay are symmetric about the wavelength $\lambda_{\max}$.

Since the dispersion d_ρ (in ps/nm) is the rate of change of delay with wavelength, we find

$$\begin{aligned} d_\rho &= \frac{d\tau_\rho}{d\lambda} \\ &= \frac{2\tau_\rho}{\lambda} - \frac{\lambda^2}{2\pi c}\frac{d^2\theta_\rho}{d\lambda^2} \\ &= -\frac{2\pi c}{\lambda^2}\frac{d^2\theta_\rho}{d\omega^2}. \end{aligned} \tag{33}$$

In a uniform grating, the dispersion is zero near $\lambda_{\max}$, and only becomes appreciable near the band edges and side lobes of the reflection spectrum, where it tends to vary rapidly with wavelength. Qualitatively, this behavior of the delay and dispersion (along with numerous other characteristics of fiber gratings) can be nicely explained by an "effective medium picture" developed by Sipe *et al.* [12]. For wavelengths outside the bandgap, the boundaries of the uniform grating (at $z = \pm L/2$) act like abrupt interfaces, thus forming a Fabry–Perot-like cavity. The nulls in the reflection spectrum are analogous to Fabry–Perot resonances—at these frequencies light is trapped inside the cavity for many round-trips, thus experiencing enhanced delay.

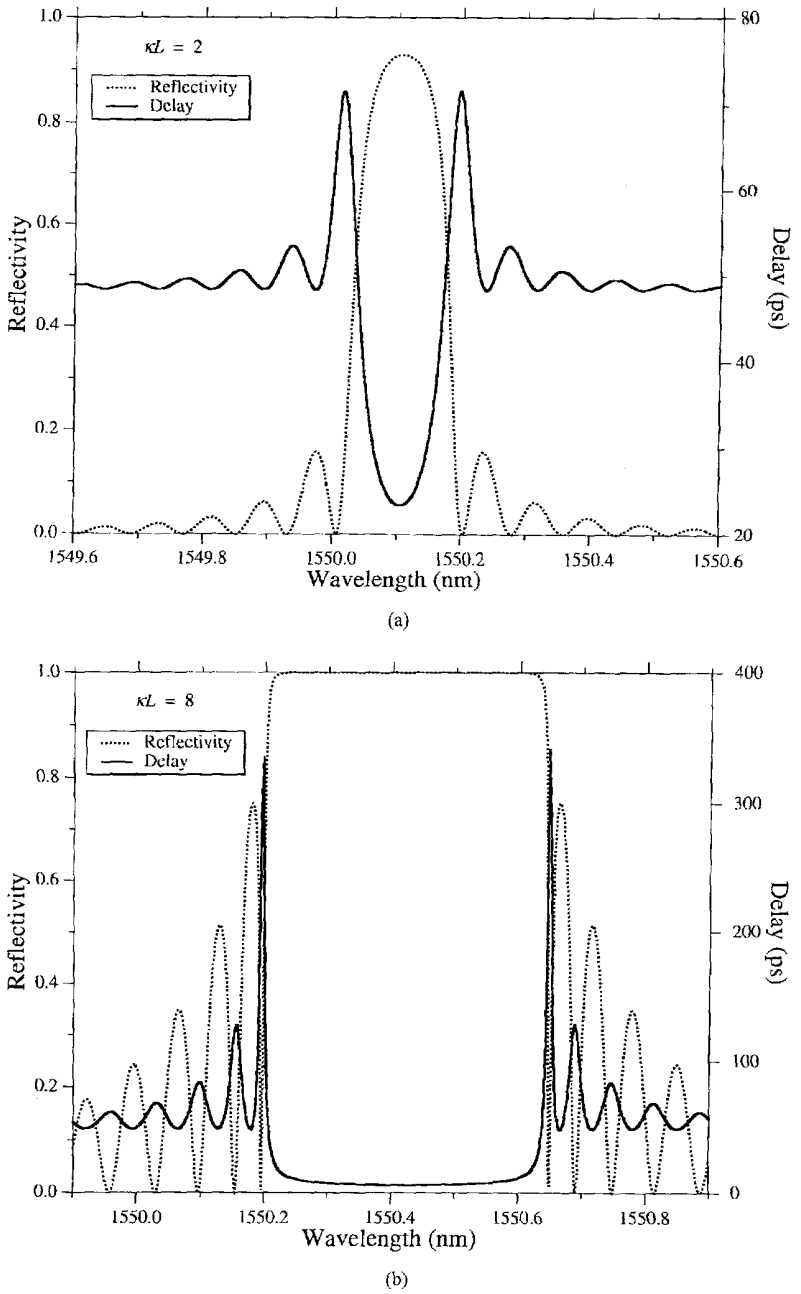

Fig. 7. Calculated reflection spectra (dotted line) and group delay (solid line) for uniform Bragg gratings with (a) $\kappa L = 2$ and (b) $\kappa L = 8$.

D. Transmission Gratings

Near the wavelength at which a mode "1" of amplitude $A_1(z)$ is strongly coupled to a co-propagating mode "2" with amplitude $A_2(z)$, (9) and (10) may be simplified by retaining only terms that involve the amplitudes of these two modes, and then making the usual synchronous approximation. The resulting equations can be written

$$\frac{dR}{dz} = i\hat{\sigma}R(z) + i\kappa S(z) \tag{34}$$

$$\frac{dS}{dz} = -i\hat{\sigma}S(z) + i\kappa^* R(z) \tag{35}$$

where the new amplitudes R and S are $R(z) \equiv A_1 \exp[-i(\sigma_{11} + \sigma_{22})z/2] \exp(i\delta z - \phi/2)$ and $S(z) \equiv A_2 \exp[-i(\sigma_{11} + \sigma_{22})z/2] \exp(-i\delta z + \phi/2)$, and where σ_{11} and σ_{22} are "dc" coupling coefficients defined in (12). In (34) and (35), $\kappa = \kappa_{21} = \kappa_{12}^*$ is the "ac" cross-coupling coefficient from (13) and $\hat{\sigma}$ is a general "dc" self-coupling coefficient defined as

$$\hat{\sigma} \equiv \delta + \frac{\sigma_{11} - \sigma_{22}}{2} - \frac{1}{2}\frac{d\phi}{dz}. \tag{36}$$

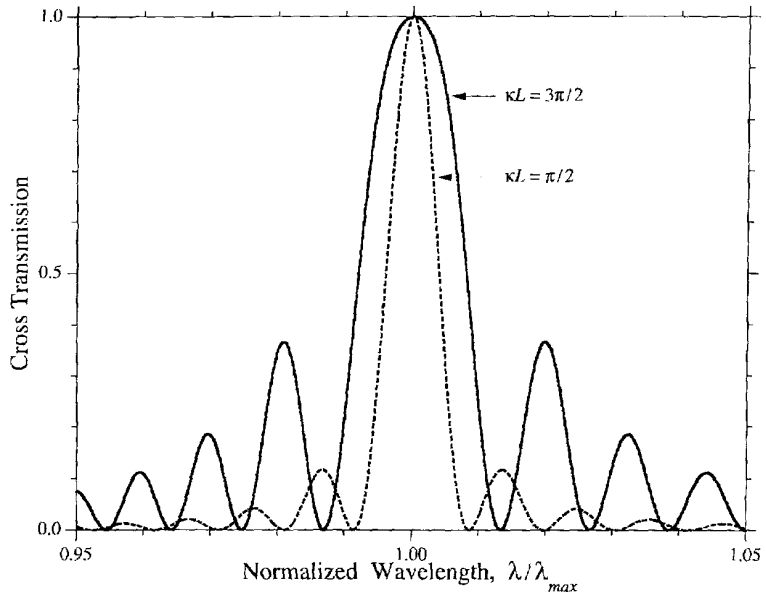

Fig. 8. Calculated cross transmission $t_\times$ through uniform transmission gratings with $\kappa L = \pi/2$ (dashed line) and $\kappa L = 3\pi/2$ (solid line).

Here the detuning, which is assumed to be constant along z, is

$$\delta \equiv \frac{1}{2}(\beta_1 - \beta_2) - \frac{\pi}{\Lambda} = \pi \Delta n_{\text{eff}} \left(\frac{1}{\lambda} - \frac{1}{\lambda_D} \right) \tag{37}$$

where $\lambda_D \equiv \Delta n_{\text{eff}} \Lambda$ is the Design wavelength for an infinitesimally weak grating. As for Bragg gratings, $\delta = 0$ corresponds to the grating condition predicted by the qualitative picture of grating diffraction, or $\lambda = \Delta n_{\text{eff}} \Lambda$.

For a uniform grating $\hat{\sigma}$ and κ are constants. Unlike for the case of Bragg reflection of a single mode, here the coupling coefficient κ generally can not be written simply as in (20). For coupling between two different modes in both Bragg and transmission gratings the overlap integrals (12) and (13) must be evaluated numerically. (For untilted gratings closed-form expressions exist, but these still require numerical evaluation of Bessel functions.) Like the analogous Bragg-grating equations, (34) and (35) are coupled first-order ordinary differential equations with constant coefficients. Thus, closed-form solutions can be found when appropriate initial conditions are specified. The transmission can be found by assuming only one mode is incident from $z = -\infty$ [say $R(0) = 1$ and $S(0) = 0$]. The power *bar* and *cross* transmission, $t_= = |R(z)|^2/|R(0)|^2$ and $t_\times = |S(z)|^2/R(0)|^2$, respectively, can be shown to be [10]

$$t_= = \cos^2\left(\sqrt{\kappa^2 + \hat{\sigma}^2} z\right) + \frac{1}{1 + \frac{\kappa^2}{\hat{\sigma}^2}} \sin^2\left(\sqrt{\kappa^2 + \hat{\sigma}^2} z\right) \tag{38}$$

$$t_\times = \frac{1}{1 + \frac{\hat{\sigma}^2}{\kappa^2}} \sin^2\left(\sqrt{\kappa^2 + \hat{\sigma}^2} z\right). \tag{39}$$

Typical examples of the cross transmission $t_\times$ for two uniform gratings of length L with $\kappa L = \pi/2$ (dashed line), $\kappa L = 3\pi/2$ (solid line), and $\sigma_{11} = \sigma_{22} = 0$ are shown in Fig. 8, plotted versus the normalized wavelength defined in (23). Here the total number of grating periods is $N = 100$. If N were larger or smaller, the bandwidth would be narrower or broader, respectively, for a given value of κL. The maximum cross transmission (which occurs when $\hat{\sigma} = 0$) is

$$t_{\times,\max} = \sin^2(\kappa L) \tag{40}$$

and it occurs at the wavelength

$$\lambda_{\max} = \frac{1}{1 - (\sigma_{11} - \sigma_{22}) \frac{\Lambda}{2\pi}} \lambda_D. \tag{41}$$

For coupling between a core mode "1" and a cladding mode "2" [see Fig. 4(b)] with an induced index change in the core only, $\sigma_{11} = \sigma$ from (19), and we find that $\sigma_{22} \ll \sigma_{11}$ (since the core confinement factor for the cladding mode is small). Therefore, we can approximate (41) as

$$\lambda_{\max} \cong \left(1 + \frac{\overline{\delta n_{\text{eff}}}}{\Delta n_{\text{eff}}}\right) \lambda_D \tag{42}$$

where we have assumed that $\overline{\delta n_{\text{eff}}}$, the induced change in the core-mode effective index, is much smaller than Δn_{eff}. Comparing (42) to (25), we see that the wavelength of maximum coupling in a long-period cladding-mode coupler grating shifts (toward longer wavelengths) as the grating is being written $n_{\text{eff}}/\Delta n_{\text{eff}}$ times more rapidly than the shift that occurs in a Bragg grating.

A useful measure of the bandwidth of a transmission grating is the separation between the first zeros on either side of the spectral peak. Looking at the excursion of $\hat{\sigma}$ from $\hat{\sigma} = 0$ that

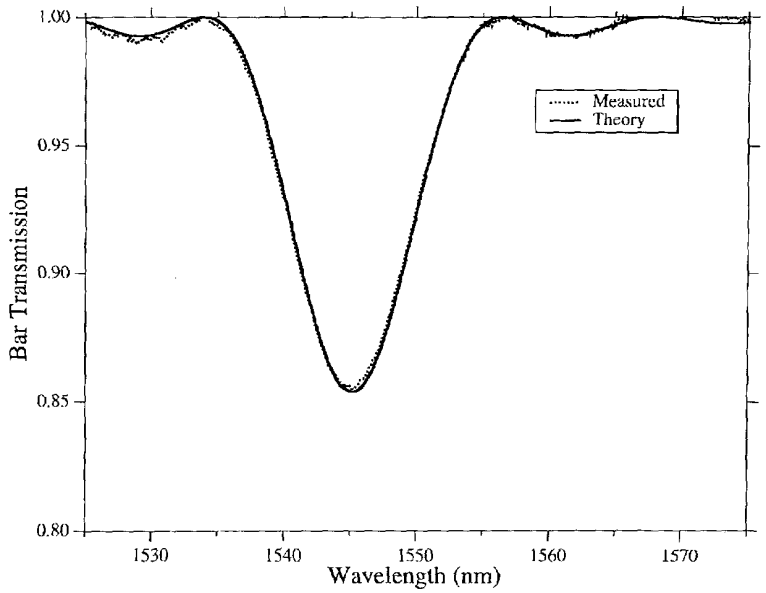

Fig. 9. Measured (dotted line) and calculated (solid line) bar transmission $t_=$ through a uniform cladding-mode transmission grating.

causes the numerator in (39) to go to zero, we find

$$\frac{\Delta\lambda_0}{\lambda} = \frac{2\lambda}{\Delta n_{\text{eff}} L}\sqrt{1-\left(\frac{\kappa L}{\pi}\right)^2} \tag{43}$$

for a grating in which at most one complete exchange of power between the two modes occurs ($\kappa L \leq \pi$). For very weak gratings the normalized bandwidth is simply $\Delta\lambda_0/\lambda = 2/N$, just as for weak Bragg gratings. For strongly overcoupled gratings where $\kappa L \gg \pi$, the sidelobes become significantly more pronounced and hence, a better measure of the bandwidth is the FWHM of the envelope traced by the peaks of the sidelobes. Looking at the first factor in the expression for $t_\times$ in (39), we find

$$\frac{\Delta\lambda_{env}}{\lambda} = \frac{2\lambda\kappa}{\pi\Delta n_{\text{eff}}}. \tag{44}$$

Since sidelobes are usually undesirable, most transmission gratings are designed such that $\kappa L \leq \pi/2$ where for the strongest gratings (large cross transmission) $\kappa L \sim \pi/2$.

To compare the theory to an experimental measurement, Fig. 9 shows the measured (dots) and calculated (line) bar transmission $t_=$ for a relatively weak grating that couples the LP_{01} core mode to the lowest-order cladding mode in a standard dispersion-shifted fiber ($\Delta n_{\text{eff}} = 0.0042$). The grating is 50 mm long and has a coupling-length product of $\kappa L = 0.39$.

Whereas, the bandwidth estimates above are generally accurate for practical Bragg gratings, the estimates (43) and (44) for transmission gratings can be poor if the effective-index dispersion is large near the resonant wavelength. The estimates assume Δn_{eff} is independent of wavelength. But if, for example, $\Delta n_{\text{eff}} \propto \lambda$ over an appreciable span of wavelengths, then from (37) the detuning δ could remain small and thus allow strong coupling over the entire span, giving rise to a much broader grating! Dispersion is more of a concern for transmission gratings mainly because these tend to have broader bandwidths than Bragg gratings even in the absence of dispersion.

While the results in this section apply rigorously only to coupling between two modes by a uniform grating, many of these "rules-of-thumb"; prove to be excellent approximations even for nonuniform gratings.

III. Two-Mode Coupling in Nonuniform Gratings

In this section, we investigate the properties of nonuniform gratings in which the coupling occurs predominantly between two modes. We consider approaches to modeling both Bragg and transmission gratings and look at examples of several types of nonuniformity.

Most fiber gratings designed for practical applications are not uniform gratings. Often the main reason for choosing a nonuniform design is to reduce the undesirable sidelobes prevalent in uniform-grating spectra; but there are many other reasons to adjust the optical properties of fiber gratings by tailoring the grating parameters along the fiber axis. It has been known for some time that apodizing the coupling strength of a waveguide grating can produce a reflection spectrum that more closely approximates the often-desired "top-hat" shape [13]–[15]. Sharp, well-defined filter shapes are rapidly becoming critical characteristics for passive components in dense wavelength-division multiplexed (DWDM) communications systems. Chirping the period of a grating enables the dispersive properties of the scattered light to be tailored [13]. Chirped fiber gratings are useful for dispersion compensation [16], for controlling and shaping short pulses in fiber lasers [17], and for creating stable continuous-wave (cw) and tunable mode-locked external-cavity semiconductor lasers [18], [19]. Sometimes it is desirable to create discrete, localized phase shifts in

an otherwise periodic grating. Discrete phase shifts can be used to open an extremely narrow transmission resonance in a reflection grating or to tailor the passive filter shape. Perhaps the most well-known application of discrete phase shifts is the use of a "quarter-wave" or π phase shift in the center of a distributed-feedback laser to break the threshold condition degeneracy for the two lowest-order laser modes, thus favoring single-mode lasing [20], [21]. Recently interest has grown in gratings with periodic superstructure, in which the coupling strength, "dc" index change, or grating period is varied periodically with a period much larger than the nominal grating period Λ. Such "sampled" gratings have been proposed and demonstrated for a number of applications [22], including use as a wavelength reference standard for DWDM systems [23]. Understanding effects of discrete phase shifts and superstructure has become critical recently with the advent of meter-long Bragg gratings for dispersion compensation produced by stitching together exposure regions formed with multiple phase masks [24], [25].

We consider two standard approaches for calculating the reflection and transmission spectra that result from two-mode coupling in nonuniform gratings. The first is direct numerical integration of the coupled-mode equations. This approach has several advantages, but it is rarely the fastest method. The second approach is a piecewise-uniform approach, in which the grating is divided into a number of uniform pieces. The closed-form solutions for each uniform piece are combined by multiplying matrixes associated with the pieces. This method is simple to implement, almost always sufficiently accurate, and generally the fastest. Other approaches are also possible, such as treating each grating half-period like a layer in a thin-film stack (Rouard's Method) [26]. Like the piecewise-uniform approach, this method amounts to multiplying a string of matrixes; but because the number of matrixes scales with the number of grating periods, this approach can become intractable for fiber gratings that are centimeters long with 10^5 periods or more.

The direct-integration approach to solving the coupled-mode equations is straightforward. The equations have been given above: (15) and (16) apply to Bragg gratings and (34) and (35) are used for transmission gratings. Likewise the boundary conditions have been described above. For a Bragg grating of length L, one generally takes $R(L/2) = 1$ and $S(L/2) = 0$, and then integrates backward from $z = L/2$ to $z = -L/2$, thus obtaining $R(-L/2)$ and $S(-L/2)$. Since the transmission grating problem is an initial-value problem, the numerical integration is done in the forward direction from $z = -L/2$ to $z = L/2$, starting with the initial conditions $R(-L/2) = 1$ and $S(-L/2) = 0$, for example. Typically, adaptive-stepsize Runge–Kutta numerical integration works well.

For modeling apodized gratings by direct numerical integration, we simply use the z-dependent quantities $\sigma_{kj}(z)$ and $\kappa_{kj}(z)$ in the coupled-mode equations, which give rise to a $\hat{\sigma}(z)$ that also depends on z. For some apodized grating shapes, we need to truncate the apodization function. For example, fiber gratings are frequently written by a Gaussian laser beam, and thus have an approximately Gaussian profile of the form

$$\overline{\delta n}_{\text{eff}}(z) = \overline{\delta n}_{\text{eff}} \exp\left(-\frac{4 \ln 2 z^2}{\text{FWHM}^2}\right) \tag{45}$$

where $\overline{\delta n}_{\text{eff}}$ is the peak value of the "dc" effective index change and FWHM is the full-width-at-half-maximum of the grating profile. Typically (45) is truncated at several times the FWHM, i.e., we choose $L \sim 3\text{FWHM}$. Another common profile is the "raised-cosine" shape

$$\overline{\delta n}_{\text{eff}}(z) = \overline{\delta n}_{\text{eff}} \frac{1}{2}\left[1 + \cos\left(\frac{\pi z}{\text{FWHM}}\right)\right]. \tag{46}$$

This profile is truncated at $L = \text{FWHM}$, where it is identically zero. Many other apodized profiles are of interest as well, such as the "flat-top raised-cosine."

Chirped gratings can be modeled using the direct integration technique by simply including a nonzero z-dependent phase term $(\frac{1}{2})d\phi/dz$ in the self-coupling coefficient $\hat{\sigma}$ defined in (17) and (36). In terms of more readily understandable parameters, the phase term for a linear chirp is

$$\frac{1}{2}\frac{d\phi}{dz} = -\frac{4\pi n_{\text{eff}} z}{\lambda_D^2}\frac{d\lambda_D}{dz} \tag{47}$$

where the "chirp" $d\lambda_D/dz$ is a measure of the rate of change of the design wavelength with position in the grating, usually given in units of nanometers/centimeters. Linear chirp can also be specified in terms of a dimensionless "chirp parameter" F [13], given by

$$\begin{aligned} F &= \frac{\text{FWHM}^2}{z^2}\phi(z) \\ &= -4\pi n_{\text{eff}}\frac{\text{FWHM}^2}{\lambda_D^2}\frac{d\lambda_D}{dz}. \end{aligned} \tag{48}$$

F is a measure of the fractional change in the grating period over the whole length of the grating. It is important to recognize that because chirp is simply incorporated into the coupled-mode equations as a z-dependent term in the self-coupling coefficient $\hat{\sigma}$, its effect is identical to that of a "dc" index variation $\sigma(z)$ with the same z dependence. This equivalence has been used to modify dispersion of gratings without actually varying the grating period [15].

Incorporating discrete phase shifts and superstructure into the direct-integration approach is straightforward. For example, as the integration proceeds along z, each time a discrete phase shift is encountered a new constant phase shift is added in the expressions (1) or (14). In the coupled-mode equations (15) and (16), we thus multiply the current value of κ by $\exp(i\phi)$ where ϕ is the shift in grating phase. Superstructure is implemented through the z dependence in $\sigma(z)$ and $\kappa(z)$. For example, for sampled gratings we simply set $\kappa = 0$ in the nongrating regions.

The often-preferred piecewise-uniform approach to modeling nonuniform gratings is based on identifying 2×2 matrices for each uniform section of the grating, and then multiplying all of these together to obtain a single 2×2 matrix that describes the whole grating [27]. We divide the grating into M uniform sections and define R_i and S_i to be the field amplitudes after traversing the section i. Thus for Bragg

gratings we start with $R_0 = R(L/2) = 1$ and $S_0 = S(L/2) = 0$ and calculate $R(-L/2) = R_M$ and $S(-L/2) = S_M$, while for transmission gratings we start with $R_0 = R(-L/2) = 1$ and $S_0 = S(-L/2) = 0$ and calculate $R(L/2) = R_M$ and $S(L/2) = S_M$. The propagation through each uniform section i is described by a matrix $\mathbf{F}_i$ defined such that

$$\begin{bmatrix} R_i \\ S_i \end{bmatrix} = \mathbf{F}_i \begin{bmatrix} R_{i-1} \\ S_{i-1} \end{bmatrix}. \tag{49}$$

For Bragg gratings the matrix $\mathbf{F}_i^B$ is given by (50) shown at the bottom of the page where Δz is the length of the ith uniform section, the coupling coefficients $\hat{\sigma}$ and κ are the local values in the ith section, and

$$\gamma_B \equiv \sqrt{\kappa^2 - \hat{\sigma}^2}. \tag{51}$$

Note γ_B is imaginary at wavelengths for which $|\hat{\sigma}| > \kappa$. For transmission gratings the matrix $\mathbf{F}_i^c$ is shown in (52) at the bottom of the page where in this case

$$\gamma_c \equiv \sqrt{\kappa^2 + \hat{\sigma}^2}. \tag{53}$$

Once all of the matrices for the individual sections are known, we find the output amplitudes from

$$\begin{bmatrix} R_M \\ S_M \end{bmatrix} = \mathbf{F} \begin{bmatrix} R_0 \\ S_0 \end{bmatrix}; \quad \mathbf{F} = \mathbf{F}_M \cdot \mathbf{F}_{M-1} \cdot \ldots \cdot \mathbf{F}_i \cdot \ldots \cdot \mathbf{F}_1. \tag{54}$$

The number of sections needed for the piecewise-uniform calculation is determined by the required accuracy. For most apodized and chirped gratings $M \sim 100$ sections is sufficient. For quasiuniform gratings like discrete-phase-shifted and sampled gratings, M is simply determined by the number of actual uniform sections in the grating. M may not be made arbitrarily large, since the coupled-mode-theory approximations that lead to (15), (16), (34), and (35) are not valid when a uniform grating section is only a few grating periods long [27]. Thus, we require $\Delta z \gg \Lambda$, which means we must maintain

$$M \ll \frac{2n_{\text{eff}}L}{\lambda_D}. \tag{55}$$

To implement the piecewise-uniform method for apodized and chirped gratings, we simply assign constant values σ, κ, and $(1/2)d\phi/dz$ to each uniform section, where these might be the z-dependent values of $\sigma(z)$, $\kappa(z)$, and $(\frac{1}{2})d\phi/dz$ evaluated at the center of each section. For phase-shifted and sampled gratings, we insert a phase-shift matrix $\mathbf{F}_{pi}$ between the factors $\mathbf{F}_i$ and $\mathbf{F}_{i+1}$ in the product in (54) for a phase shift after the ith section. For Bragg gratings the phase-shift matrix is of the form

$$\mathbf{F}_{pi}^B = \begin{bmatrix} \exp\left(\frac{-i\phi_i}{2}\right) & 0 \\ 0 & \exp\left(\frac{i\phi_i}{2}\right) \end{bmatrix} \tag{56}$$

and for transmission gratings $\mathbf{F}_{pi}^c = (\mathbf{F}_{pi}^B)^*$, since we propagate the field amplitudes in the $-z$ direction for Bragg gratings but the $+z$ direction for transmission gratings. Here, ϕ_i is the shift in the phase of the grating itself for discrete phase shifts, and for sampled gratings [see Fig. 2(f)]

$$\frac{\phi_i}{2} = \frac{2\pi n_{\text{eff}}}{\lambda} \Delta z_0 \tag{57}$$

where Δz_0 is the separation between two grating sections.

Having described two basic approaches for calculating reflection and transmission spectra through nonuniform gratings, we now give several examples that demonstrate the effects of apodization, chirp, phase shifts, and superstructure on the optical properties of fiber gratings. For most of the examples in the remainder of this section the piecewise-uniform method was used because of its speed, but the results are indistinguishable from those obtained by direct integration.

To demonstrate the effects of apodization, Fig. 10 shows the reflection and group delay versus wavelength for gratings similar to those described in Fig. 7, only here the gratings have a Gaussian profile as illustrated in Fig. 2(b) and described by (45). The maximum index change values $\overline{\delta n}_{\text{eff}}$ and the FWHM = 1 cm for the gratings in Fig. 10(a) and (b) are the same as the uniform index change values and the length of the uniform gratings in Fig. 7(a) and (b), respectively. We see that the spectra are similar, except there are no sidelobes on the long-wavelength side and very different sidelobes on the short-wavelength side of the Gaussian spectra. The short-wavelength structure is caused by the nonuniform "dc" index change and has been described in detail elsewhere [12], [28]. Short wavelengths lie inside the local band gap ($|\hat{\sigma}| < \kappa$) associated with the wings of the grating and thus are strongly reflected there, but lie outside the local band gap near the center of the grating where they are only weakly reflected; the wings of the grating thus act like a Fabry–Perot cavity at short

$$\mathbf{F}_i^B = \begin{bmatrix} \cosh(\gamma_B\Delta z) - i\frac{\hat{\sigma}}{\gamma_B}\sinh(\gamma_B\Delta z) & -i\frac{\kappa}{\gamma_B}\sinh(\gamma_B\Delta z) \\ i\frac{\kappa}{\gamma_B}\sinh(\gamma_B\Delta z) & \cosh(\gamma_B\Delta z) + i\frac{\hat{\sigma}}{\gamma_B}\sinh(\gamma_B\Delta z) \end{bmatrix} \tag{50}$$

$$\mathbf{F}_i^c = \begin{bmatrix} \cos(\gamma_c\Delta z) + i\frac{\hat{\sigma}}{\gamma_c}\sin(\gamma_c\Delta z) & i\frac{\kappa}{\gamma_c}\sin(\gamma_c\Delta z) \\ i\frac{\kappa}{\gamma_c}\sin(\gamma_c\Delta z) & \cos(\gamma_c\Delta z) - i\frac{\hat{\sigma}}{\gamma_c}\sin(\gamma_c\Delta z) \end{bmatrix} \tag{52}$$

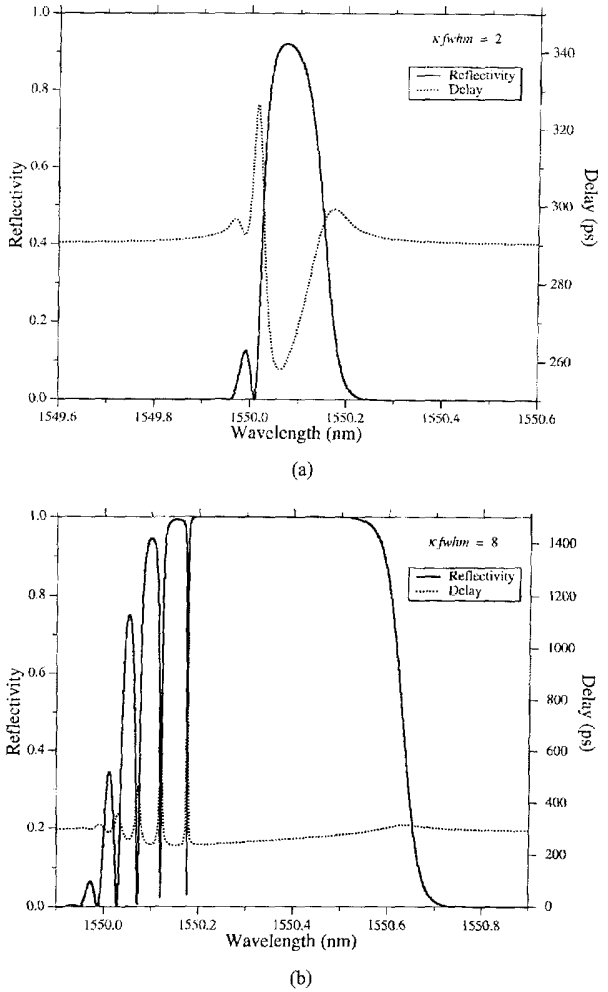

Fig. 10. Reflection and group delay versus wavelength for Gaussian gratings similar to the uniform gratings in Fig. 7: (a) κFWHM = 2 and (b) κFWHM = 8.

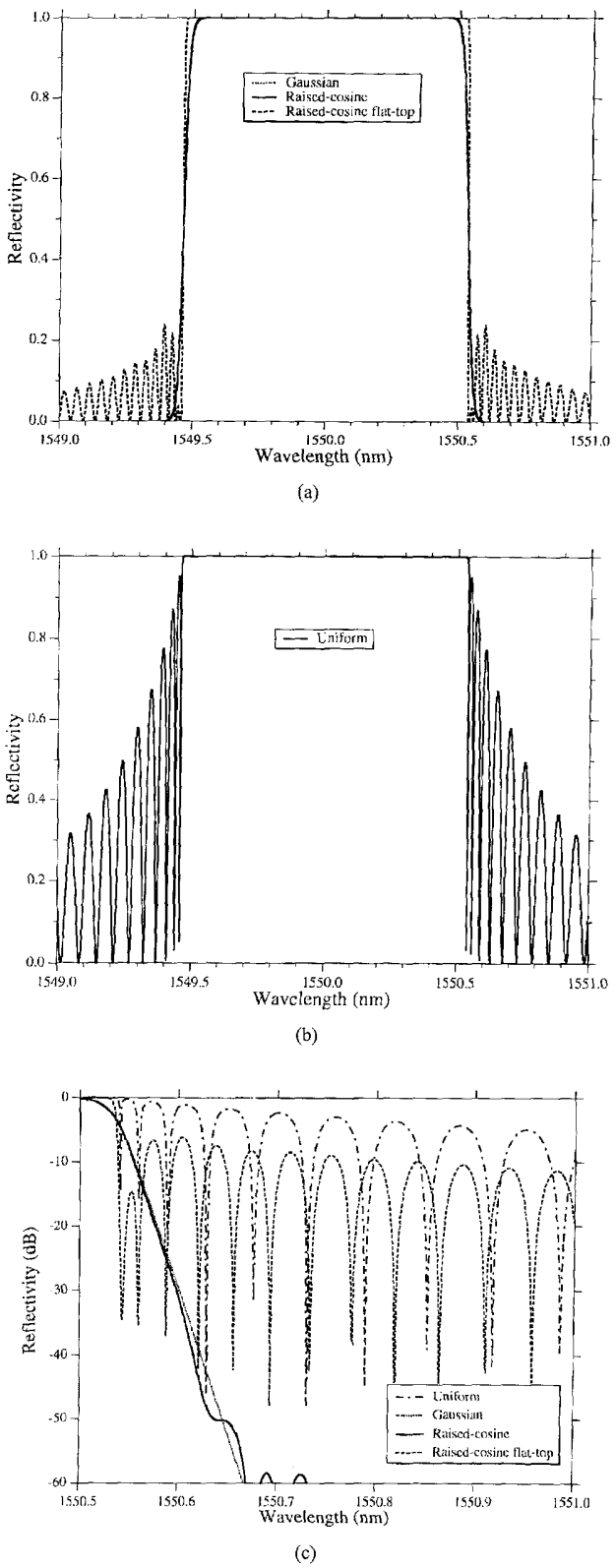

Fig. 11. Calculated reflectivity of uniform and nonuniform gratings with "ac" index change of 1×10^{-3}, zero "dc" index change, and FWHM = 10 mm. (a) Gaussian (dotted line), raised-cosine (solid line), and flat-top raised-cosine (dashed line), (b) uniform grating, and (c) expanded view of filter edge in dB.

wavelengths. Note that the difference in nonresonant delay (at wavelengths far from the Bragg resonance) between Figs. 7 and 10 is not significant. The *relative* delay is more relevant than the absolute delay, which is sensitive to the identification of time zero (or $z = L/2$ in this case).

In Fig. 11(a) the reflection spectra for several nonuniform gratings are plotted, where for each the "dc" index change is assumed to be zero ($\sigma \rightarrow 0$), as illustrated in Fig. 2(c). In the models described above the "dc" index change is set to a small value ($\overline{\delta n}_{\text{eff}} \rightarrow 0$) while the "ac" index change is maintained at the desired value, here $v\overline{\delta n}_{\text{eff}} = 1 \times 10^{-3}$, by assuming a large fringe visibility $v \rightarrow \infty$. The grating profiles include a Gaussian, a raised-cosine, and a flat-top raised-cosine (in which the length of the uniform region is twice the FWHM of the cosine region) with the total FWHM = 10 mm for each. The Gaussian and raised-cosine gratings are indistinguishable on this plot. Note that the side lobes on the short-wavelength side of the Gaussian and raised-cosine spectra (see Fig. 10) have been eliminated by making the "dc" index change uniform, and the spectra are

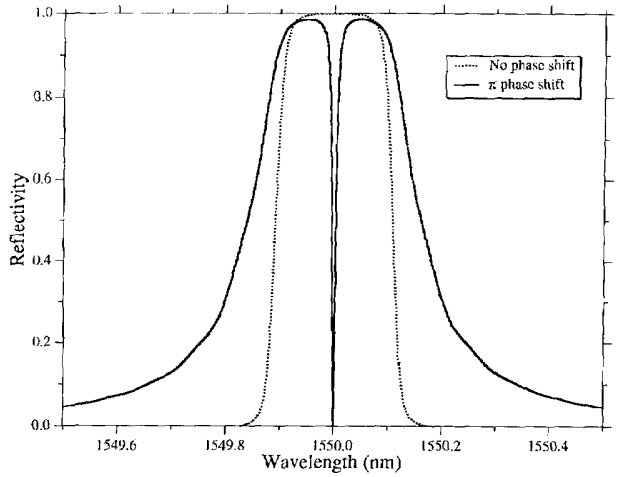

Fig. 12. Calculated reflectivity of a raised-cosine grating with (solid line) and without (dotted line) a π phase shift in the phase of the grating at the center.

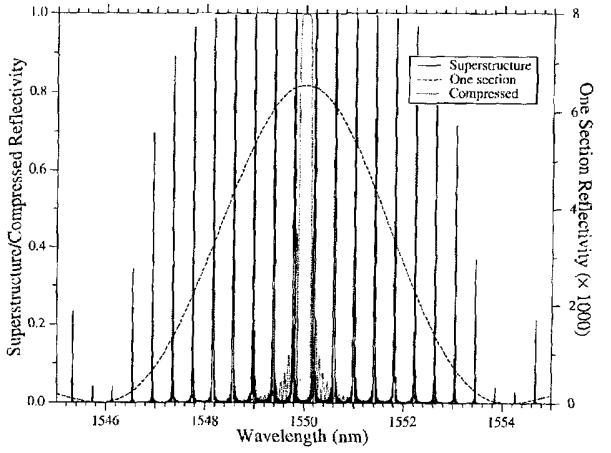

Fig. 13. Calculated reflectivity of a uniform grating with periodic superstructure (solid line) where the 100-mm-long grating has 50 200-μm-long grating sections spaced 1.8 mm apart. Also shown are the reflectivity of a single 200-μm-long section (dashed line) and of the compressed grating (dotted line), in which the 1.8 mm grating-free sections are removed.

symmetric about $\lambda_{\max}$. For comparison Fig. 11(b) shows a 10-mm-long uniform grating with zero "dc" index change. To investigate how well the apodized gratings approximate a "top-hat" spectrum, Fig. 11(c) shows a close-up view of the filter edges on a logarithmic scale. The (minimal) differences between the Gaussian and raised-cosine gratings are evident here; although the inherently truncated raised-cosine does exhibit side lobes, they are below −50 dB.

An example of gratings with (solid line) and without (dotted line) a discrete phase shift are shown in Fig. 12. The gratings have a raised-cosine shape with FWHM = 10 mm, maximum "ac" index change $v\overline{\delta n}_{\text{eff}} = 2 \times 10^{-4}$, and no "dc" index change ($\overline{\delta n}_{\text{eff}} \to 0$). The π phase shift of the grating phase at the center opens a narrow transmission resonance at the design wavelength, but also broadens the reflection spectrum and diminishes $r_{\max}$.

The reflection spectrum of a sampled grating exhibiting periodic superstructure is shown in Fig. 13 (solid line). As illustrated in Fig. 2(f), the grating is uniform except for regions where $v\overline{\delta n}_{\text{eff}}$ is set to zero. Here, the "ac" index change in the nonzero regions is $v\overline{\delta n}_{\text{eff}} = 5 \times 10^{-4}$, the total length of the grating is 100 mm, and there are 50 sections with an "on–off" duty cycle of 10%. To facilitate an understanding of the resulting spectrum, the dashed line in Fig. 13 shows the reflection spectrum produced by a single section of this grating with the same index change; since its length is 200 μ m, $\kappa L = 0.2$ for this section. The zeros in the envelope of the sampled-grating spectrum coincide with the zeros of the single-section spectrum. Also shown in this figure (dotted line) is a plot of the spectrum that results when the sampled grating is "compressed," such that the total length of the modulated portion of the grating is maintained (10 mm), but the unmodulated regions are removed.

An example of a chirped grating is shown in Fig. 14. The grating has a "zero-dc" raised-cosine profile with FWHM = 1 cm, $v\overline{\delta n}_{\text{eff}} = 5 \times 10^{-4}$, and a chirp of $d\lambda_D/dz = -1$ nm/cm. The plot shows the group delay calculated from

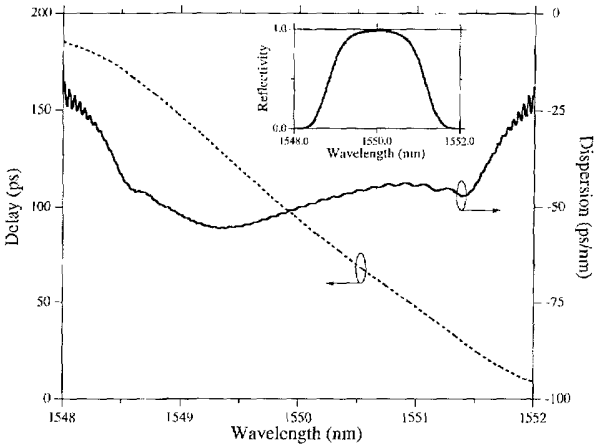

Fig. 14. Calculated group delay (dashed line) and dispersion (solid line) of a raised-cosine grating with "ac" index change of 5×10^{-4}, zero "dc" index change, FWHM = 10 mm, and a chirp of −1 nm/cm. The inset shows the reflectivity spectrum.

(32) (dashed line), the dispersion calculated from (33) (solid line), and the reflection spectrum (inset). The bandwidth of a similar, unchirped grating estimated from (31) is 0.53 nm. A commonly used estimate of dispersion in a linearly chirped grating when variation of grating period along z is the dominant source of chirp is

$$d_\rho \sim 100\left(\frac{d\lambda_D}{dz}\right)^{-1} (\text{ps/nm}) \tag{58}$$

where $d\lambda_D/dz$ is in units nm/cm, and we have approximated $2n_{\text{eff}}/c \cong 100$ ps/cm. According to (58), the grating in Fig. 14 should exhibit a dispersion of $d_\rho = -100$ ps/nm and thus a delay of $\tau_\rho = 200$ ps between 1549–1551 nm. These simple estimates disagree with the actual values by almost a factor of two, mainly because the effective chirp resulting from apodization is comparable to the grating-period chirp.

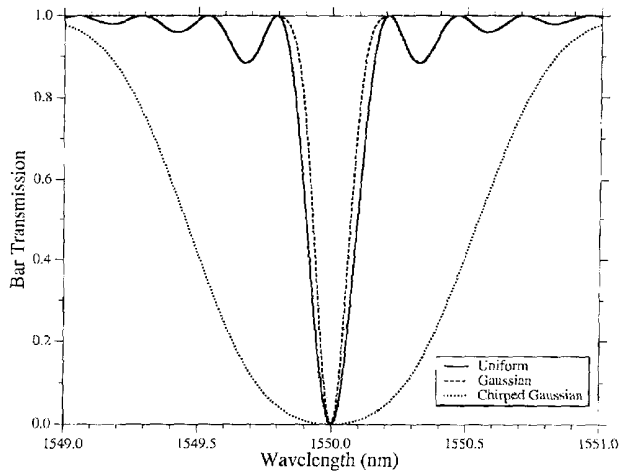

Fig. 15. Calculated bar transmission $t_=$ through a uniform grating (solid line), a Gaussian grating (dashed line), and a chirped Gaussian grating (dotted line) with grating parameters given in the text.

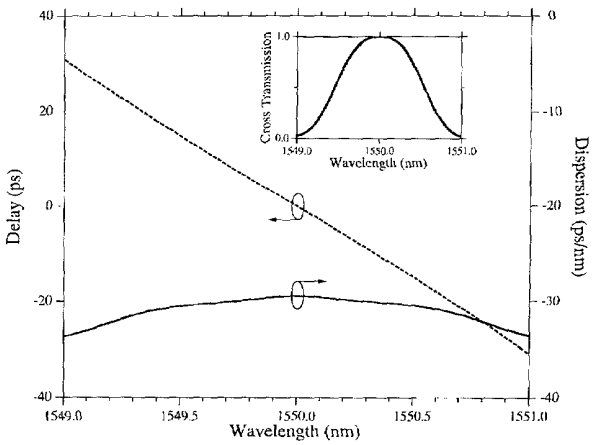

Fig. 16. Group delay and dispersion for the cross amplitude of light transmitted through the chirped Gaussian grating described in Fig. 15. Cross transmission $t_\times$ is shown in the inset.

Several examples of bar-transmission spectra through nonuniform transmission gratings are shown in Fig. 15. The solid line shows transmission through a uniform grating with a coupling-length product of $\kappa L = \pi/2$, "zero-dc" index change ($\sigma_{11} = \sigma_{22} = 0$), an effective-index difference of $\Delta n_{\text{eff}} = 0.1$, and a length of 10 cm. The dashed line represents the transmission through a similar grating but with a Gaussian profile where the coupling-length product has been slightly reduced to $\kappa \cdot \text{FWHM} = 0.48\pi$ to maintain maximum coupling. Note the reduction of the side lobes, just as occurs for Bragg gratings. Although no example is shown, if the "dc" index change were nonzero, as shown in Fig. 2(b), the Gaussian grating spectrum would exhibit "Fabry–Perot" structure on the short-wavelength side of the spectrum similar to that shown in Fig. 10. The dotted line in Fig. 15 is the transmission spectrum obtained for a similar Gaussian grating with a linear chirp of $d\lambda_D/dz = -0.025$ nm/cm and $\kappa \cdot \text{FWHM} = 1.4\pi$. Fig. 16 shows the spectrum of the group delay and dispersion associated with this grating; the cross transmission is shown in the inset. Although the dispersion is relatively small for this example, note how linear the delay is over the full bandwidth of the grating.

IV. Tilted Gratings

Another parameter the designer of fiber gratings has at his disposal is the tilt of the grating fringes in the core of the fiber [29], [30]. The main effect of grating tilt in a single-mode Bragg grating is to effectively reduce the fringe visibility v defined in (1), (13), and (14). However, grating tilt can also dramatically affect the coupling to radiation modes, which we discuss briefly in Section VI, as well as enable otherwise unallowed coupling between discrete bound modes of fiber. The latter interaction has been demonstrated in both Bragg [31] and transmission gratings [32] that couple the LP_{01} mode to the LP_{11} mode of a dual-mode fiber.

To see how grating tilt affects single-mode Bragg reflection in a fiber grating, suppose that the induced index change in the

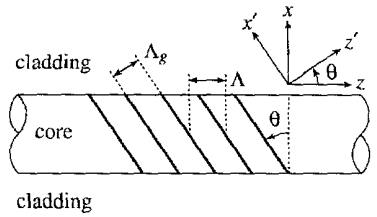

Fig. 17. Diagram of the parameters associated with a tilted phase grating in the core of an optical fiber.

core of the fiber δn_{co} is rotated by an angle θ, such that it is

$$\delta n_{co}(x, z) = \overline{\delta n}_{co}(z')\left\{1 + v\cos\left[\frac{2\pi}{\Lambda_g}z' + \phi(z')\right]\right\} \quad (59)$$

where the z'-axis, shown in Fig. 17, is defined to be $z' = x\sin\theta + z\cos\theta$. The grating period along the z (fiber) axis, which determines the resonant wavelengths for coupling, is thus $\Lambda = \Lambda_g/\cos\theta$. For the slowly varying functions $\overline{\delta n}_{co}(z')$ and $\phi(z')$, we take $z' \cong z\cos\theta$; i.e., we simply take the projection of these functions onto the fiber axis. The general coupling coefficient in (14) then becomes

$$K^t_{\mp\pm}(z) = \sigma(z) + 2\kappa_{\mp\pm}(z)\cos\left[\frac{2\pi}{\Lambda}z + \phi(z\cos\theta)\right] \quad (60)$$

where we recognize that the subscripts j and k describe the same mode, except when one is associated with the forward-going mode (+) the other describes the backward-going mode (−). The self and cross coupling coefficients now become

$$\sigma(z) = \frac{\omega n_{co}}{2}\overline{\delta n}_{co}(z\cos\theta)\iint_{\text{core}} dx\,dy\,\vec{e}_{\mp t}(x, y) \cdot \vec{e}^{\,*}_{\pm t}(x, y) \quad (61)$$

and

$$\kappa_{\mp\pm}(z, \theta) = \frac{v}{2}\frac{\omega n_{co}}{2}\overline{\delta n}_{co}(z\cos\theta)\iint_{\text{core}} dx\,dy \cdot \exp\left(\pm i\frac{2\pi}{\Lambda}x\tan\theta\right)\vec{e}_{\mp t}(x, y) \cdot \vec{e}^{\,*}_{\pm t}(x, y). \quad (62)$$

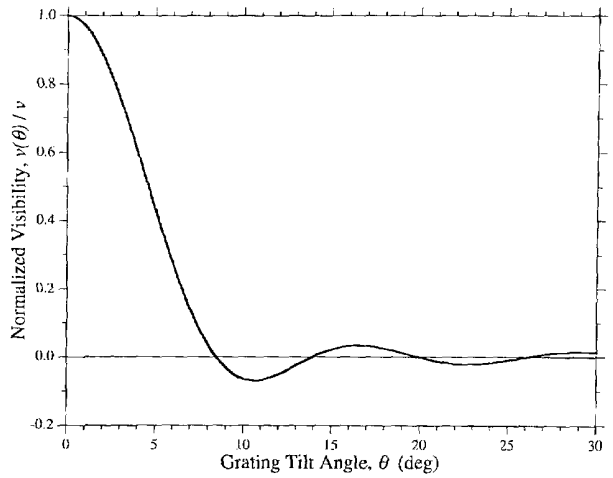

Fig. 18. Plot of the normalized effective fringe visibility associated with single-mode Bragg reflection in a tilted grating in the core of a fiber with parameters described in the text.

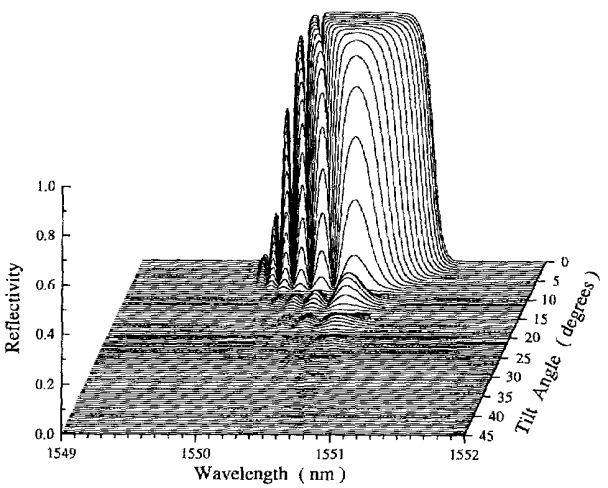

Fig. 19. Calculated reflectivity spectrum over a range of grating tilt angles for a Gaussian grating.

Notice that $\kappa_{+-} = (\kappa_{-+})^*$. Except for scaling of the slowly varying functions, the effects of tilt can be lumped into an "effective fringe visibility" $v_{\mp\pm}(\theta)$, defined such that

$$\frac{v_{\mp\pm}(\theta)}{v} = \frac{\displaystyle\iint_{\text{core}} dx\,dy \exp\left(\pm i\frac{2\pi}{\Lambda}x\tan\theta\right)\vec{e}_{\mp t}(x,y)\cdot\vec{e}^{\,*}_{\pm t}(x,y)}{\displaystyle\iint_{\text{core}} dx\,dy\,\vec{e}_{\mp t}(x,y)\cdot\vec{e}^{\,*}_{\pm t}(x,y)}. \tag{63}$$

Therefore, we may write

$$\kappa_{\mp\pm}(z,\theta) = \frac{v_{\mp\pm}(\theta)}{2}\sigma(z) \tag{64}$$

in direct analogy to (13). This important result states that the effect of grating tilt on single-mode Bragg reflection is simply to reduce the effective fringe visibility by an amount given in (63). As an example, Fig. 18 shows a plot of the normalized effective fringe visibility as a function of tilt angle θ for the LP_{01} mode in a fiber with a cladding index of 1.44, a core-cladding $\Delta = 0.0055$, a core radius of $a = 2.625$ μm, and at a wavelength of 1550 nm.

The Bragg reflection spectrum for a tilted grating can still be calculated from (15) and (16) where now $\kappa \equiv \kappa_{-+}$. Fig. 19 shows reflection spectra over a range of tilt angles for a Gaussian grating with a FWHM = 5 mm, a maximum index change of $\overline{\delta n}_{\text{eff}} = 7.25 \times 10^{-4}$, and zero-tilt visibility $v = 1$. Because tilt affects Bragg reflection by effectively reducing the fringe visibility, this plot also demonstrates how the reflection spectrum of a Gaussian grating changes as the visibility is reduced (here by keeping the "dc" index change constant). Proper use of tilt for reducing the effective visibility and hence, Bragg reflection can be practically useful in cases where large radiation or other bound mode coupling is desired but Bragg reflection is undesirable [31].

V. Coupling to Cladding Modes

There are numerous applications of fiber gratings that involve coupling of light into and out of the core mode(s) of a fiber. Fig. 20 shows measured spectra of the transmission of an LP_{01} core mode through an untilted Gaussian fiber grating that is 5 mm long and has a maximum index change of $\overline{\delta n}_{\text{eff}} = 2 \times 10^{-3}$. In Fig. 20(a) the bare (uncoated) section of fiber that contains the grating is immersed in index-matching fluid to simulate an infinite cladding. What results is a smooth transmission profile for $\lambda < 1540$ nm demonstrating loss due to coupling of the core mode to the continuum of radiation modes. Radiation mode coupling is briefly discussed in Section VI and is described in detail in [28] and [29]. In Fig. 20(b), the fiber is immersed in glycerin, which has a refractive index greater than the cladding index. The transmission spectrum now exhibits fringes that are caused by Fabry–Perot-like interference resulting from partial reflection of the radiation modes off of the cladding–glycerin interface. In Fig. 20(c) the bare fiber is surrounded by air; for the wavelengths shown in this plot, the LP_{01} core mode couples into distinct backward-going cladding modes with a well-defined resonance peak for each mode. Here we briefly examine this last type of interaction. A more detailed description can be found in [33].

Fig. 4(b) illustrates coupling of a core mode to a cladding mode from a ray point-of-view, where cladding modes are bound modes of the total fiber with $1 \le n_{\text{eff}} \le n_{cl}$ (assuming the fiber is surrounded by air). It is shown above that the grating period required for co-propagating coupling between a core mode of index n_{eff}^{co} and a cladding mode of index n_{eff}^{cl} is $\Lambda = \lambda/(n_{\text{eff}}^{co} - n_{\text{eff}}^{cl})$. In analogous fashion, counter-propagating modes [$\theta_2 < 0$ in Fig. 4(b)] can be coupled by a grating with a much shorter period $\Lambda = \lambda/(n_{\text{eff}}^{co} + n_{\text{eff}}^{cl})$.

Using the coupled-mode theory outlined above, the equations that describe coupling among the LP_{01} core mode and the (exact) cladding modes of order 1μ by a reflection grating

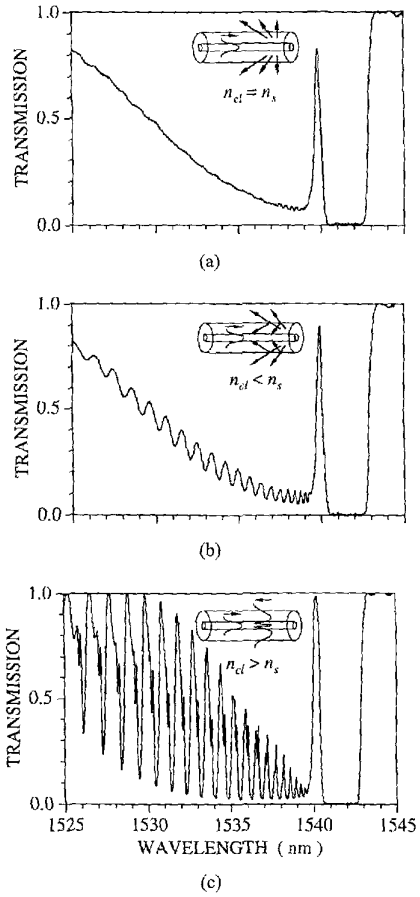

Fig. 20. Measured transmission through a Bragg grating where (a) the uncoated fiber is immersed in index-matching liquid to simulate an infinite cladding, (b) the fiber is immersed in glycerin, and (c) the bare fiber is surrounded by air and thus supports cladding modes.

are [33]

$$\frac{dA^{co}}{dz} = i\sigma_{01-01}^{co-co}A^{co} + i\sum_{\mu}\kappa_{1\mu-01}^{cl-co}B_{\mu}^{cl}\exp\left(-i2\delta_{1\mu-01}^{cl-co}z\right) \tag{65}$$

$$\sum_{\mu}\left[\frac{dB_{\mu}^{cl}}{dz} = -i\kappa_{1\mu-01}^{cl-co}A^{co}\exp\left(+i2\delta_{1\mu-01}^{cl-co}z\right)\right] \tag{66}$$

where the detuning is

$$\delta_{1\mu-01}^{cl-co} \equiv \frac{1}{2}\left(\beta_{01}^{co} + \beta_{1\mu}^{cl} - \frac{2\pi}{\Lambda}\right). \tag{67}$$

Here, σ_{01-01}^{co-co} is the self-coupling coefficient for the LP_{01} mode given by (19), $\kappa_{1\mu-01}^{cl-co}$ is the cross-coupling coefficient defined through (12) and (13), and we have neglected terms that involve self and cross coupling between cladding modes since the associated coupling coefficients are very small, or $\sigma_{1\mu-1\mu}^{cl-cl}$, $\kappa_{1\mu-1\nu}^{cl-cl} \ll \kappa_{1\mu-01}^{cl-co} \ll \sigma_{01-01}^{co-co}$. In (65) and (66), we have also not included Bragg reflection of the LP_{01} core mode, making these equations valid only at wavelengths far away from this Bragg resonance.

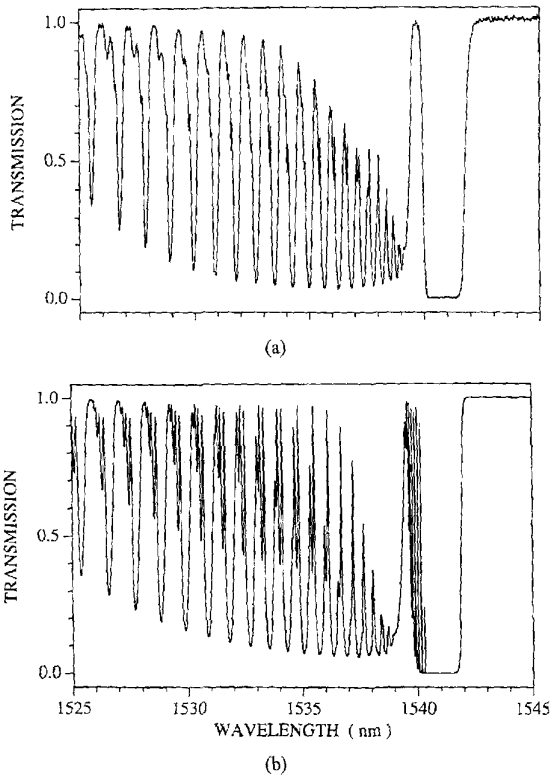

Fig. 21. (a) Measured and (b) calculated transmission through a strong Gaussian Bragg grating, showing both core-mode Bragg reflection into cladding modes.

The common synchronous approximation was used in obtaining (65) and (66), but unlike (15) and (16) the resulting equations contain coefficients that oscillate rapidly along z. This is because there are now multiple values of δ, which are not easily removed by defining R and S as we did for (15) and (16). However, if the cladding mode resonances do not overlap, then we may calculate each resonance separately, retaining only the core mode and the appropriate cladding mode for the resonance. In that case, the problem reduces to simple two-mode coupling, as described in detail in Sections II and III.

As an example of cladding-mode coupling in a Bragg grating, Fig. 21 shows the measured (a) and calculated (b) transmission spectrum through a Gaussian grating written in hydrogen-loaded [34] Corning Flexcore fiber. The grating length is FWHM = 4 mm, the index change is $\overline{\delta n}_{\text{eff}} = 2.8 \times 10^{-3}$, and the visibility is approximately $v = 1$. The large transmission dip at 1541 nm is the Bragg reflection resonance, while the remaining dips are cladding mode resonances. Here the resonances overlap substantially over most of the wavelength range shown in the plot. As a result, an accurate calculation could be obtained only by including multiple (but not necessarily all) cladding modes in (65) and (66) at each wavelength. The resolution in the experimental measurement is 0.1 nm.

The equations that describe coupling among the LP_{01} core mode and the cladding modes of order 1 μ by a transmission

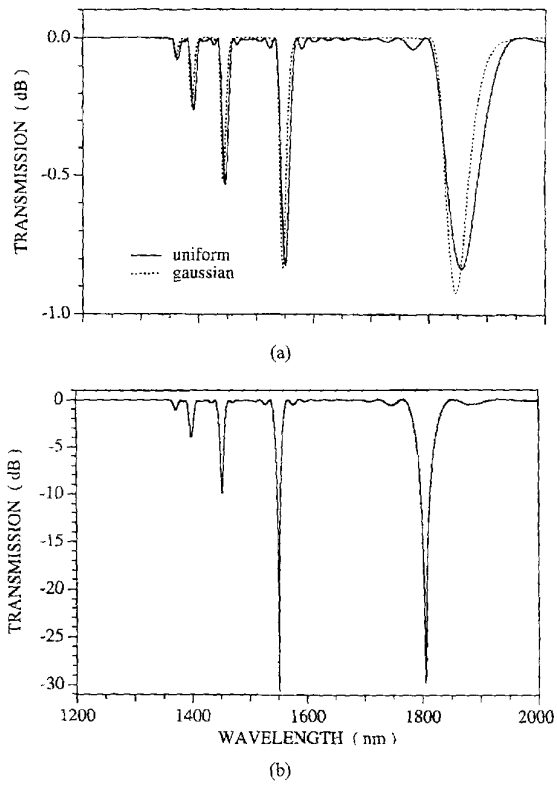

Fig. 22. Calculated transmission spectra through (a) a relatively weak and (b) a stronger transmission grating, each designed to couple the LP_{01} core mode to the $\mu = 7$ cladding mode at 1550 nm. Solid lines represent a uniform grating while the dashed line represents a Gaussian grating.

grating are [33]

$$\frac{dA^{co}}{dz} = i\sigma_{01-01}^{co-co}A^{co} + i\sum_{\mu}\kappa_{1\mu-01}^{cl-co}A_{\mu}^{cl}\exp\left(-i2\delta_{1\mu-01}^{cl-co}z\right) \tag{68}$$

$$\sum_{\mu}\left[\frac{dA_{\mu}^{cl}}{dz} = +i\kappa_{1\mu-01}^{cl-co}A^{co}\exp\left(+i2\delta_{1\mu-01}^{cl-co}z\right)\right] \tag{69}$$

$$\delta_{1\mu-01}^{cl-co} \equiv \frac{1}{2}\left(\beta_{01}^{co} - \beta_{1\mu}^{cl} - \frac{2\pi}{\Lambda}\right). \tag{70}$$

In arriving at (68) and (69), approximations were applied similar to those made for (65) and (66). Fig. 22 shows calculated examples of cladding-mode coupling in a transmission grating. Fig. 22(a) shows the transmission for a relatively weak grating with a length (FWHM) of 25 mm, a maximum index change of $\overline{\delta n}_{\text{eff}} = 2 \times 10^{-4}$, and a uniform (solid line) or Gaussian (dashed line) profile. The four main dips seen in these spectra correspond to coupling to the $\mu = 1$, 3, 5, 7, and 9 cladding modes. Fig. 22(b) shows the transmission for a stronger, uniform grating with an induced index change of 1×10^{-3}. In each case the grating period is adjusted to achieve coupling at 1550 nm between the LP_{01} core mode and the $\mu = 5$ cladding mode. That is, the gratings in Fig. 22(a) and (b) have periods of $\Lambda = 545$ μm and $\Lambda = 502$ μm, respectively.

In the above discussion we consider only the $l\mu$ cladding modes with azimuthal order $l = 1$. In an untilted grating coupling may occur only between modes of the same azimuthal symmetry (as shared by the $LP_{01} = HE_{11}$ mode and the exact $HE/EH_{1\mu}$ cladding modes). In a typical 125-μm diameter fiber there are several hundred $l = 1$ cladding modes at IR communications wavelengths. In a tilted grating, in which coupling to an enormous number of higher azimuthal-order cladding modes is allowed, the resonances are so densely spaced that they are generally not well resolvable.

VI. Radiation-Mode Coupling

Although numerous applications are possible for fiber gratings as waveguide-grating couplers that couple free-space beams into and out of bound fiber modes, surprisingly little work has been reported in this area. However, the effect of radiation-mode coupling as a loss mechanism on core-mode transmission has been studied [28], [29]. We do not describe this situation in detail, but merely introduce the reader to the main concepts in order to put radiation-mode coupling in context with the interactions discussed above.

Fig. 23 illustrates the coupling of an LP_{01} core mode to the continuum of backward propagating radiation modes from a ray point of view. The coupling strength to these high-order (small-θ_2) modes is quite small unless the grating is suitably blazed. But as Fig. 20(a) illustrates, if the fiber is immersed in an index matching fluid or recoated with a high-index polymer, bound cladding modes cease to exist and substantial coupling to low-order ($|\beta_2| > 2\pi/\lambda$) radiation modes can occur near the Bragg reflection resonance even in untilted gratings. A useful quantity to be aware of is the wavelength λ_{cut} at which true radiation-mode (not cladding-mode) coupling "cuts" on and/or off. Assuming the core confinement factor for the radiation modes is much smaller than that of the bound mode of interest, then we find

$$\lambda_{\text{cut}} \cong \frac{1}{2}\left(1 \pm \frac{n}{n_{\text{eff}}}\right)\left(1 + \frac{\overline{\delta n}_{\text{eff}}}{n_{\text{eff}}}\right)\lambda_D \tag{71}$$

where $n = n_{cl}$ for the case of an infinitely clad fiber with index n_{cl} [see Fig. 20(a)], or $n = 1$ when the fiber is surrounded by air such that bound cladding modes may propagate. The "+" sign in the first factor applies to reflection, while the "−" sign corresponds to forward coupling. The second factor describes the shift of λ_{cut} with increasing "dc" index change.

Consider the coupling of an LP_{01} core mode to backward-propagating radiation modes labeled $LP_{p\rho}$, where the discrete index p identifies the polarization and azimuthal order, while the continuous label $\rho = \sqrt{(2\pi/\lambda)^2 n_{cl}^2 - \beta_{p\rho}^2}$ denotes the transverse wavenumber of the radiation mode ($\beta_{p\rho}$ is the usual axial propagation constant). Here we assume the fiber has a cladding of index n_{cl} and with an infinite radius. The coupled-mode equations for this case are then

$$\frac{dA}{dz} = i\sigma_{01-01}^{co-co}A + i\sum_{p}\int d\rho\,\kappa_{p\rho-01}^{ra-co}B_{p\rho} \cdot \exp\left(-i2\delta_{p\rho-01}^{ra-co}z\right) \tag{72}$$

$$\frac{dB_{p\rho}}{dz} = -i\kappa_{01-p\rho}^{co-ra}A\exp\left(+i2\delta_{p\rho-01}^{ra-co}z\right) \tag{73}$$

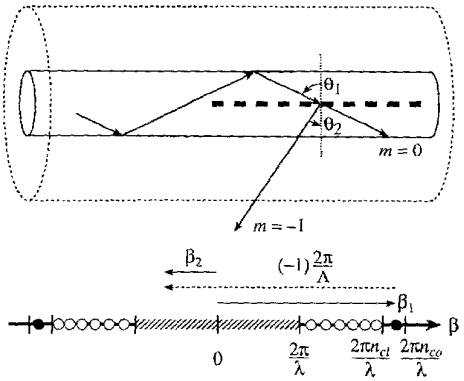

Fig. 23. Ray-optic illustration of core-mode coupling to a backward-traveling radiation mode by a Bragg grating. The β axes below the diagram demonstrates the grating condition in (5) for $m = 1$.

where

$$\delta_{p\rho-01}^{ra-co} \equiv \frac{1}{2}\left(\beta_{01} + \beta_{p\rho} - \frac{2\pi}{\Lambda}\right) \tag{74}$$

and where A is the amplitude of the core mode, $B_{p\rho}$ are the amplitudes of the (continuous spectrum of) radiation modes, and the usual summation now includes an integral in (72). Also, σ_{01-01}^{co-co} is the LP_{01} self-coupling coefficient given by (19), and $\kappa_{01-p\rho}^{co-ra} = (\kappa_{p\rho-01}^{ra-co})^*$ is the cross-coupling coefficient defined through (12) and (13). By applying essentially a "first Born approximation" to the core-mode amplitude A, we can obtain an approximate expression for $B_{p\rho}$ from (73). After inserting this result into (72) and performing the integral over ρ, it can be shown [28], [29] that the core mode amplitude approximately obeys an equation of the form

$$\frac{dA}{dz} = i\sigma_{01-01}^{co-co}A - \left[\sum_p \frac{\pi\beta_{p\rho}}{\rho}|\kappa_{p\rho-01}^{ra-co}|^2\right]A \tag{75}$$

where the term in square brackets is evaluated at $\beta_{p\rho} = 2\pi/\Lambda - \beta_{01}$. Since this term is real, clearly it gives rise to exponential loss in the amplitude of the core mode. Notice the loss coefficient is proportional to the square of the cross-coupling coefficient, and hence, to the square of the induced index change.

Although the analysis given here is simplified, it is possible to predict the radiation-mode coupling loss spectrum even when the grating is tilted following a similar development to that in Section IV. As might be expected, as the tilt angle is increased (the grating is blazed), light can be coupled more efficiently at smaller angles $|\theta_2|$. But increasingly many radiation-mode azimuthal orders must be included in the summation in (75) to accurately model radiation modes propagating more normal to the fiber axis. As an example of some typical transmission spectra, Fig. 24 shows a calculation of the loss in transmission through the same Gaussian grating described in Fig. 19, only here $\overline{\delta n}_{\text{eff}} = 1.5 \times 10^{-3}$. Spectra are shown for a range of tilt angles between 0 –45°, where the grating period Λ along the fiber axis is kept constant. The LP_{01} mode incident on the grating is assumed to be polarized perpendicular to both the x and z axes (see Fig. 17). The

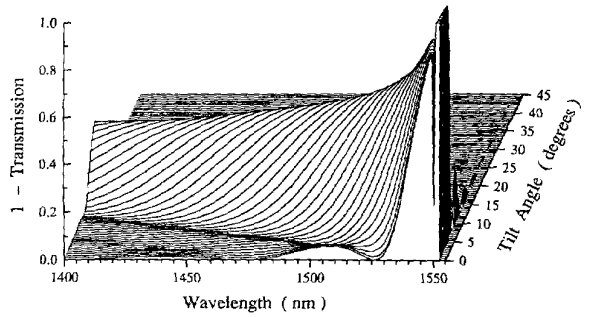

Fig. 24. Calculated loss in transmission through a Gaussian grating in a fiber with an infinite cladding over a range of grating tilt angles.

peak at the longest wavelength results from Bragg reflection, whereas the loss at other wavelengths is due to radiation-mode coupling. As expected, the efficiency for coupling to smaller and smaller angles θ_2 (which occurs at shorter wavelengths) improves as the grating is increasingly blazed.

VII. Conclusions

We have presented principles and tools for understanding the spectra exhibited by fiber Bragg and transmission gratings. It is hoped that the reader less familiar with these exciting components now has a base with which to understand the current and potential applications of fiber gratings, and that the more experienced reader has benefited from a concise description of multiple fiber-grating phenomena with a uniform notation.

An important principle to take away from Section II is that the simple closed-form expressions for optical properties of uniform fiber gratings are frequently excellent approximations for nonuniform gratings as well. This section also uncovers some of the basic similarities and differences between Bragg gratings and transmission gratings. One important difference is that as a Bragg grating is made increasingly stronger (by enlarging $\overline{\delta n}_{\text{eff}}$), the maximum reflectivity and bandwidth simply increase; in contrast, to obtain a strong resonance in a transmission grating requires hitting a "target" $\overline{\delta n}_{\text{eff}}$ (usually $\kappa L = \pi/2$) to avoid over-coupling.

By examining nonuniform gratings in Section III, we found that it is critical to take into account both apodization and chirp of the grating period when the dispersive characteristics of fiber gratings are important. We also saw that it is almost always advantageous to minimize the "dc" apodization, unless it is intentionally utilized for tailoring dispersion, for example. In Section IV, we found that tilted gratings enable coupling between modes that have dissimilar azimuthal symmetry, and that the effect of tilt on single-mode Bragg reflection can be regarded simply as a reduction in the effective fringe visibility of the phase grating. Finally, in Sections V and VI, we briefly explored coupling from a core mode to cladding and radiation modes. Although long-period cladding-mode coupling gratings have recently seen rapid development [35], there appears to be relatively little investigation into the apparently abundant possibilities for applications based on exchange of light in the core of a single-mode fiber with the readily accessible cladding and radiation modes.

ACKNOWLEDGMENT

The author would like to thank the Editors of this Special Section for the invitation to present this paper and the referees for their helpful comments.

REFERENCES

[1] K. O. Hill, B. Malo, F. Bilodeau, and D. C. Johnson, "Photosensitivity in optical fibers," *Annu. Rev. Mater. Sci.*, vol. 23, pp. 125–157, 1993.
[2] W. W. Morey, G. A. Ball, and G. Meltz, "Photoinduced Bragg gratings in optical fibers," *Opt. Photon. News*, vol. 5, pp. 8–14, 1994.
[3] R. J. Campbell and R. Kashyap, "The properties and applications of photosensitive germanosilicate fiber," *Int. J. Optoelectron.*, vol. 9, pp. 33–57, 1994.
[4] P. St. J. Russell, J.-L. Archambault, and L. Reekie, "Fiber gratings," *Phys. World*, pp. 41–46, Oct. 1993.
[5] I. Bennion, J. A. R. Williams, L. Zhang, K. Sugden, and N. J. Doran, "UV-written in-fiber Bragg gratings," *Opt. Quantum Electron.*, vol. 28, pp. 93–135, 1996.
[6] Invited Papers, *J. Lightwave Technol.*, this issue.
[7] C. M. de Sterke, N. G. R. Broderick, B. J. Eggleton, and M. J. Steel, "Nonlinear optics in fiber gratings," *Opt. Fiber Tech.*, vol. 2, pp. 253–268, 1996.
[8] D. Marcuse, *Theory of Dielectric Optical Waveguides*. New York: Academic, 1991, ch. 2.
[9] M. Born and E. Wolf, *Principles of Optics*. New York: Pergamon, 1987, sec. 8.6.1, eq. (8).
[10] A. Yariv, "Coupled-mode theory for guided-wave optics," *IEEE J. Quantum Electron.*, vol. QE-9, pp. 919–933, 1973.
[11] H. Kogelnik, "Theory of optical waveguides," in *Guided-Wave Optoelectronics*, T. Tamir, Ed. New York: Springer-Verlag, 1990.
[12] J. E. Sipe, L. Poladian, and C. M. de Sterke, "Propagation through nonuniform grating structures," *J. Opt. Soc. Amer. A*, vol. 11, pp. 1307–1320, 1994.
[13] H. Kogelnik, "Filter response of nonuniform almost-periodic structures," *Bell Sys. Tech. J.*, vol. 55, pp. 109–126, 1976.
[14] K. O. Hill, "Aperiodic distributed-parameter waveguides for integrated optics," *Appl. Opt.*, vol. 13, pp. 1853–1856, 1974.
[15] B. Malo, S. Theriault, D. C. Johnson, F. Bilodeau, J. Albert, and K. O. Hill, "Apodised in-fiber Bragg grating reflectors photoimprinted using a phase mask," *Electron. Lett.*, vol. 31, pp. 223–225, 1995.
[16] F. Ouellette, "Dispersion cancellation using linearly chirped Bragg grating filters in optical waveguides," *Opt. Lett.*, vol. 12, pp. 847–849, 1987.
[17] M. E. Fermann, K. Sugden, and I. Bennion, "High-power soliton fiber laser based on pulse width control with chirped fiber Bragg gratings," *Opt. Lett.*, vol. 20, pp. 172–174, 1995.
[18] P. A. Morton, V. Mizrahi, T. Tanbun-Ek, R. A. Logan, P. J. Lemaire, H. M. Presby, T. Erdogan, S. L. Woodward, J. E. Sipe, M. R. Phillips, A. M. Sergent, and K. W. Wecht, "Stable single mode hybrid laser with high power and narrow linewidth," *Appl. Phys. Lett.*, vol. 64, pp. 2634–2636, 1994.
[19] P. A. Morton, V. Mizrahi, P. A. Andrekson, T. Tanbun-Ek, R. A. Logan, P. Lemaire, D. L. Coblentz, A. M. Sergent, K. W. Wecht, and P. F. Sciortino, Jr., "Mode-locked hybrid soliton pulse source with extremely wide operating frequency range," *IEEE. Photon. Technol. Lett.*, vol. 5, pp. 28–31, 1993.
[20] H. A. Haus and C. V. Shank, "Antisymmetric taper of distributed-feedback lasers," *IEEE J. Quantum Electron.*, vol. QE-12, pp. 532–539, 1976.
[21] W. H. Loh and R. I. Laming, "1.55 μm phase-shifted distributed feedback fiber laser," *Electron. Lett.*, vol. 31, pp. 1440–1442, 1995.
[22] B. J. Eggleton, P. A. Krug, L. Poladian, and F. Ouellette, "Long periodic superstructure Bragg gratings in optical fibers," *Electron. Lett.*, vol. 30, pp. 1620–1622, 1994.
[23] J. Martin, M. Tetu, C. Latrasse, A. Bellemare, and M. A. Duguay, "Use of a sampled Bragg grating as an in-fiber optical resonator for the realization of a referencing optical frequency scale for WDM communications," in *Optical Fiber Communications Conf.*, Dallas, TX, Feb. 16–21, 1997, paper ThJ5.
[24] R. Kashyap, H.-G. Froehlich, A. Swanton, and D. J. Armes, "1.3 m long super-step-chirped fiber Bragg grating with a continuous delay of 13.5 ns and bandwidth 10 nm for broadband dispersion compensation," *Electron. Lett.*, vol. 32, pp. 1807–1809, 1996.
[25] L. Dong, M. J. Cole, M. Durkin, M. Ibsen, and R. I. Laming, "40 Gbit/s 1.55 μm transmission over 109 km of nondispersion shifted fiber with long continuously chirped fiber gratings," in *Optic. Fiber Commun. Conf.*, Dallas, TX, Feb. 16–21, 1997, paper PD6.
[26] L. A. Weller-Brophy, "Analysis of waveguide gratings: Application of Rouard's method," *J. Opt. Soc. Amer. A*, vol. 2, pp. 863–871, 1985.
[27] M. Yamada and K. Sakuda, "Analysis of almost-periodic distributed feedback slab waveguides via a fundamental matrix approach," *Appl. Opt.*, vol. 26, pp. 3474–3478, 1987.
[28] V. Mizrahi and J. E. Sipe, "Optical properties of photosensitive fiber phase gratings," *J. Lightwave Technol.*, vol. 11, pp. 1513–1517, 1993.
[29] T. Erdogan and J. E. Sipe, "Tilted fiber phase gratings," *J. Opt. Soc. Amer. A*, vol. 13, pp. 296–313, 1996.
[30] R. Kashyap, R. Wyatt, and R. J. Campbell, "Wideband gain flattened erbium fiber amplifier using a photosensitive fiber blazed grating," *Electron. Lett.*, vol. 29, pp. 154–156, 1993.
[31] T. A. Strasser, J. R. Pedrazzani, and M. J. Andrejco, "Reflective mode conversion with UV-induced phase gratings in two-mode fiber," in *Optic. Fiber Commun. Conf.*, Dallas, TX, Feb. 16–21, 1997, paper FB3.
[32] K. O. Hill, B. Malo, K. A. Vineberg, F. Bilodeau, D. C. Johnson, and I. Skinner, "Efficient mode conversion in telecommunication fiber using externally written gratings," *Electron. Lett.*, vol. 26, pp. 1270–1272, 1990.
[33] T. Erdogan, "Cladding-mode resonances in short and long period fiber grating filters," *J. Opt. Soc. Amer. A*, vol. 14, no. 8, Aug. 1997.
[34] P. J. Lemaire, R. M. Atkins, V. Mizrahi, K. L. Walker, K. S. Kranz, and W. A. Reed, "High pressure H_2 loading as a technique for achieving ultrahigh UV photosensitivity and thermal sensitivity in GeO_2 doped optical fibers," *Electron. Lett.*, vol. 29, pp. 1191–1193, 1993.
[35] A. M. Vengsarkar, P. J. Lemaire, J. B. Judkins, V. Bhatia, T. Erdogan, and J. E. Sipe, "Long-period fiber gratings as band-rejection filters," *J. Lightwave Technol.*, vol. 14, pp. 58–65, 1996.

Turan Erdogan (S'90–M'92) received the B.S. degrees in physics and electrical engineering from the Massachusetts Institute of Technology, Cambridge, in 1987, and the Ph.D. degree from The Institute of Optics at the University of Rochester, Rochester, NY, in 1992. His doctoral research focused on novel approaches to surface-emitting semiconductor lasers, including concentric-circle-grating surface-emitting lasers, and optical physics of diffraction gratings and cavities.

Until 1994, he was with AT&T Bell Laboratories in Murray Hill, NJ, where he conducted research and development of fiber grating-based devices for advanced optical communications systems. In 1994, he joined the Faculty of The Institute of Optics, Rochester, NY, as an Assistant Professor, where he continues to conduct research on fiber and semiconductor devices, including fiber gratings.

Dr. Erdogan is an Alfred P. Sloan Research Fellow, a recipient of an NSF Faculty Early Career Development (CAREER) Award, and winner of the 1995 Adolph Lomb Medal of the Optical Society of America.